Cell Reports

Article

The ventral CA2 region of the hippocampus and its differential contributions to social memory and social aggression

Graphical abstract

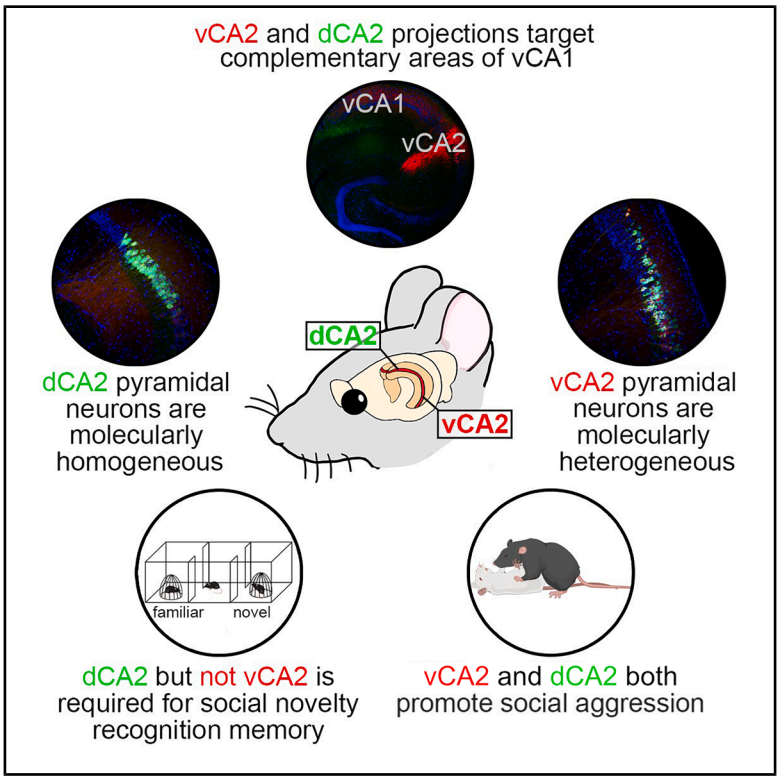

Highlights

- CA2 extends to the extreme temporal pole of the hippocampus
- Ventral CA2 differs from dorsal CA2 in projection pattern and synaptic action
- Similar to prior studies, inhibition of dorsal CA2 reduces both social memory and aggression
- In contrast, inhibition of ventral CA2 impacts social aggression but not social memory

Authors

Lara M. Boyle, Wanhui Sheng, Andres Villegas, ..., W.Scott Young, Felix Leroy, Steven A. Siegelbaum

Correspondence

sas8@cumc.columbia.edu

In brief

While studies show that hippocampal dorsal CA2 influences social memory and aggression, the characteristics of ventral CA2 are unknown. Boyle et al. show that a molecularly, anatomically, and electrophysiologically defined CA2 extends along the hippocampal septotemporal axis, with similarities and important differences in projection patterns, synaptic actions, and behavioral role.

Boyle et al., 2025, Cell Reports *44*, 115714
May 27, 2025
https://doi.org/10.1016/j.celrep.2025.115714

CellPress

Cell Reports

CellPress
OPEN ACCESS

Article

The ventral CA2 region of the hippocampus and its differential contributions to social memory and social aggression

Lara M. Boyle,[1,2,7,9] Wanhui Sheng,[2,7] Andres Villegas,[1] Rhea Sahai,[1] Sarah Irfan,[3] Heon-Jin Lee,[4,10] W.Scott Young,[4] Felix Leroy,[1,11] and Steven A. Siegelbaum[1,2,5,6,8,12,*]

[1]Department of Neuroscience, Vagelos College of Physicians and Surgeons, Columbia University Irving Medical Center, New York, NY 10027, USA
[2]Zuckerman Mind Brain Behavior Institute, Columbia University, New York, NY 10027, USA
[3]Barnard College, New York, NY 10027, USA
[4]National Institute of Mental Health, National Institutes of Health, Bethesda, MD 20892, USA
[5]Department of Pharmacology, Vagelos College of Physicians and Surgeons, Columbia University Irving Medical Center, New York, NY 10032, USA
[6]Kavli Institute for Brain Science, Columbia University, New York, NY 10027, USA
[7]These authors contributed equally
[8]Senior author
[9]Present address: University of Pennsylvania Health System, Philadelphia, PA 19104, USA
[10]Present address: Department of Microbiology and Immunology, School of Dentistry, Kyungpook National University, Daegu 41940, South Korea
[11]Present address: Instituto de Neurociencias CSIC-UMH, San Juan de Alicante, Spain
[12]Lead contact
*Correspondence: sas8@cumc.columbia.edu
https://doi.org/10.1016/j.celrep.2025.115714

SUMMARY

The dorsal and ventral regions of the CA1 field of the hippocampus play distinct roles in the encoding of cognitive vs. emotional behaviors, respectively. Whether this distinction applies to other hippocampal fields and other behaviors is unclear. Here, we focus on the hippocampal CA2 field and compare the properties and behavioral roles of its dorsal (dCA2) and ventral (vCA2) regions. Although dCA2 is known to be required for social memory and to promote social aggression, the role of vCA2 is unknown. We report that a defined CA2 region extends to the extreme ventral pole of the hippocampus, with certain distinctions to dCA2. Unlike dCA2, chemogenetic silencing of vCA2 pyramidal neurons did not impair social memory. Similar to dCA2, vCA2 was required to promote social aggression. Thus, consistent with the CA1 region, CA2 may be differentially tuned to support cognitive compared with emotional processes along its dorsal to ventral axis.

INTRODUCTION

A key goal of hippocampal research is to elucidate whether and how the distinct hippocampal subregions along both its transverse (dentate gyrus, CA3, CA2, and CA1)[1] and longitudinal (dorsal and ventral) axes differentially contribute to declarative memory. Although most studies have focused on the different transverse subregions, it is now clear that dorsal and ventral regions of the hippocampus differ in their gene expression, connectivity, and behavioral role.[2] A comprehensive RNA sequencing study of the hippocampus found that the transcriptional distance between dorsal and ventral CA1, CA3, and DG are approximately as large as those seen between the different transverse subfields.[3]

Functionally, the dorsal region of the hippocampus has been linked to more cognitive functions, including contextual and spatial memory.[4,5] In contrast, the ventral hippocampus is more important for affective behaviors such as anxiety and emotional processing.[6–9] These different behavioral roles are reflected in marked differences in the extrahippocampal projections from dorsal and ventral CA1.[2] Thus, whereas dorsal CA1 (dCA1) projects mainly to subiculum, entorhinal cortex, and lateral septum, ventral CA1 (vCA1) uniquely projects to prefrontal cortex, nucleus accumbens, amygdala, and hypothalamus.

The distinction between the behavioral roles of the dorsal and ventral hippocampus is of particular interest for social memory. Although the importance of the hippocampus for social memory has been evident since the studies by Brenda Milner and her colleagues of patient H.M.,[10] the relative importance of dorsal and ventral hippocampus remains somewhat unclear. Whereas silencing of dorsal CA1,[11] dorsal CA3,[12] or dorsal dentate gyrus[13] does not impair social novelty recognition memory (SNRM), the behavioral discrimination of a novel from familiar conspecific, silencing of ventral CA1[11] and ventral CA3[12] suppresses SNRM recall and encoding, respectively.

Although the results on CA1 and CA3 suggest a selective role for the ventral hippocampus in social memory, a number of studies have found that the dorsal CA2 (dCA2) region is critically important for encoding, consolidation, and recall of social memories.[14–21] Moreover, the contribution of dCA2 to SNRM is mediated, at least in part, through its projections to vCA1.[17] dCA2 also acts to enhance social aggression through its projection to dorsal lateral septum.[22] However, to date, all published studies of the behavioral role of CA2 have focused on its dorsal portion. Indeed, despite descriptions of ventral CA2 (vCA2) by Lorenté de Nó[1] and others,[23–25] the existence of vCA2 has been a matter of controversy.[26]

The CA2 region was first identified based on the distinct morphology of the pyramidal neurons (PNs) in this region from those in flanking CA1 and CA3 regions.[1] dCA2 PNs also have distinct electrophysiological and synaptic properties and a distinct gene expression profile relative to neighboring dCA1 and dCA3 neurons.[27–29] Of particular note, dCA2 PNs are highly enriched in receptors for the social neuropeptides arginine vasopressin (AVP)[30] and oxytocin (OXT),[31] which contribute to the regulation of social behaviors. Thus, general deletion of the gene encoding the arginine vasopressin receptor 1b (*Avpr1b*)[32] or the oxytocin receptor[31] impairs social memory, as does the conditional deletion of both receptors when restricted to CA2.[20] In addition, general deletion of *Avpr1b* inhibits social aggression[32] and this phenotype can be rescued by selective viral expression of Avpr1b in dCA2 and nearby neurons,[33] indicating that AVP acting on Avpr1b expressed by dCA2 neurons is necessary to promote normal levels of aggression.

The identification of CA2 PNs in more ventral regions of the hippocampus has been less clear cut and has relied mostly on gene expression patterns. Although certain dCA2 markers, including PCP4[24,25] and Avpr1b,[25] have been found to extend into ventral hippocampus, other markers are not as reliably expressed.[26,30,34] Based on *in situ* hybridization data from the Allen Brain Atlas, CA2 was suggested to be restricted to the dorsal two-thirds of the hippocampus and to be absent from the ventral one-third of the hippocampus.[35] However, a more recent analysis of *in situ* hybridization and single-cell mRNA expression data from the Allen Brain Atlas and DropViz databases suggested that the expression of at least a subset of CA2 markers may extend farther toward the ventral pole,[36] although the pattern of molecular expression in vCA2 neurons may be different from their dorsal counterparts.[36] At present, little is known as to the electrophysiological properties and synaptic connectivity of putative CA2 neurons in the most ventral region of hippocampus, including whether such neurons share the characteristic properties of dCA2. Importantly, the behavioral role of vCA2, and whether it participates in social behaviors as defined for dCA2, remains unexplored. Here, we provide anatomical, molecular, electrophysiological, and behavioral evidence that a defined CA2 region extends throughout the hippocampal dorsal-ventral axis using two mouse lines that provide for relatively selective Cre-dependent AAV-mediated expression in CA2, the *Avpr1b-Cre*$^{+/-}$ line[25] and the *PCP4-Cre*$^{+/-}$ line (RBRC05662, developed by Toshitada Takemori and provided by RIKEN BRC). We found that vCA2 PNs exhibited similar cellular anatomical features and electrophysiological properties to dCA2 neurons, despite a greater molecular heterogeneity in vCA2. Similar to dCA2, vCA2 is required to promote social aggression. However, unlike dCA2, vCA2 is not required for SNRM.

RESULTS

The boundaries of CA2 extend along the entire dorsoventral hippocampus

Given the differing reports on the existence of vCA2, noted above, a question arises: how should CA2 be defined in the hippocampus? Here, we define CA2 PNs as having the following features: (1) anatomical location between CA1 and CA3, with partial overlap with the end of the mossy fiber inputs from dentate gyrus; (2) lack of thorny excrescences that characterize CA3 PNs; (3) restricted or enriched expression of genes and/or proteins not expressed in CA1 or CA3, including RGS14, STEP, and/or Avpr1b[37]; and (4) distinct electrophysiological properties that differ from CA1 or CA3.[28,29]

We first explored the anatomical location of CA2 PNs based on the expression of tdTomato in the *Avprb1-Cre*$^{+/-}$ x *Ai14* tdTomato reporter line. We found that tdTomato was expressed along the entire extent of the hippocampal dorsoventral axis at a position along the transverse axis between CA3 and CA1 (Figure 1). We quantified the density of Avpr1b-expressing tdTomato+ neurons in the anatomically defined CA2 region as the fraction of DAPI-positive cells (Figure 2). There was a significantly smaller fraction of tdTomato+ cells in the CA2 region located in the ventral hippocampus (38.0% ± 5.3% of DAPI-labeled cells) compared with the dorsal hippocampus (73.5% ± 7.8% of cells; two-sample unpaired t test $t = 8.616$, $df = 9$, $p < 0.0001$), confirming previous qualitative observations.[25] Light-sheet microscopy of iDISCO[38] cleared brains confirmed that Avpr1b was expressed in a continuous band from the most dorsal to the most ventral portions of the hippocampus (Figure S1). *In situ* hybridization in *Avpr1b-Cre*$^{+/-}$ × *Ai14* mouse brains ($n = 2$), using probes against *Avpr1b* and *tdTomato* mRNAs in coronal sections, revealed that Cre-driven expression accurately reflected Avpr1b mRNA expression throughout the hippocampal longitudinal axis (Figure S2), similar to prior results in the dorsal hippocampus.[25]

To determine whether Cre-dependent expression in vCA2 PNs was associated with the expression of other classic dCA2 pyramidal cell markers, we performed immunohistochemistry for RGS14, PCP4, and STEP along the dorsoventral axis in two cohorts of *Avpr1b-Cre*$^{+/-}$ × *Ai14* mice. We selected slices from the dorsal hippocampus (first one-third of dissected hippocampus) and ventral hippocampus (last one-third of dissected hippocampus) from each subject for staining. In one cohort (mouse $n = 3$), we co-stained slices for RGS14, PCP4, and the nuclear marker DAPI (Figure 2). In another cohort (mouse $n = 4$), we co-stained slices for STEP, PCP4, and DAPI (Figure S3A). Furthermore, since PCP4 labels the dentate gyrus and mossy fiber tract, we confirmed that vCA2, like dCA2, has an anatomical localization with partial overlap of the distal end of the mossy fiber inputs (Figure S4). A consistent region was defined within the dorsal and ventral CA2 to standardize comparison of positive cell counts across these regions (see STAR Methods). This area

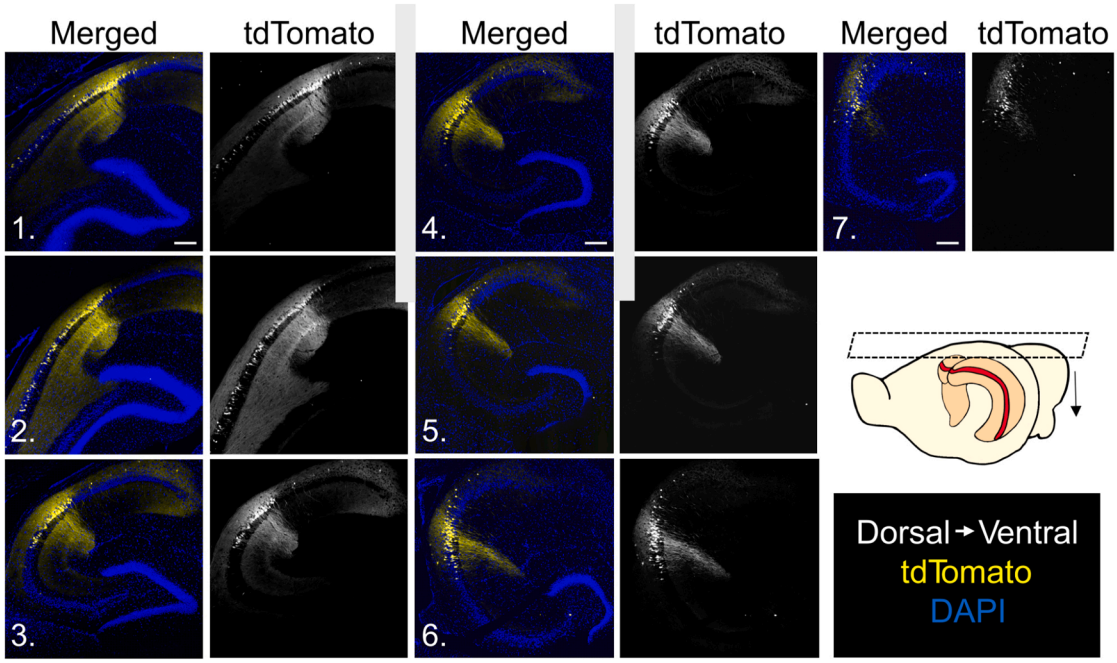

Figure 1. Horizontal slices from *Avpr1b*-Cre$^{+/-}$ x *Ai14* mice reveal tdTomato expression along the entire dorsoventral axis

tdTomato (Avpr1b) expression was present along the entire axis from the most dorsal (1) to most ventral (7) slices. Numbers on images correspond to arrows in inset. Scale bar, 200 μm.

(Figure S4) was selected because >50% of DAPI-stained neurons within this boundary express the putative CA2 marker PCP4. We quantified the total number of cells in the region that were co-labeled by at least one putative CA2 marker and DAPI (Figure 2).

In dorsal hippocampus, there was near complete overlap between all molecular markers for CA2 examined, including *Avpr1b-Cre*$^{+/-}$ dependent marker expression, as previously noted.[25] Like the *Avpr1b-Cre*$^{+/-}$ × *Ai14* reporter results noted above, the percentage of DAPI-expressing cells in the anatomically defined CA2 region in the ventral hippocampus that expressed at least one of the examined endogenous CA2 markers (61.0% ± 2.8%) was significantly less than in the dorsal hippocampus (73.6% ± 6.9%, Mann-Whitney $p = 0.0025$). Moreover, whereas the percentage of tdTomato-expressing cells in dCA2 (73.5% ± 7.8%) was nearly identical to the percentage of dCA2 cells expressing any of the other CA2 markers (73.6% ± 6.9%), significantly fewer cells in vCA2 expressed tdTomato (38.0% ± 5.3%) than the percentage of cells that expressed any of the various markers examined (61.0% ± 2.8%). These results provide evidence for a subpopulation of tdTomato-negative (i.e., *Avpr1b*-negative) vCA2 cells that expressed at least one or more of the other CA2 markers (Figure S5).

To further characterize the molecular differences between dCA2 and vCA2, we quantified the number of cells that co-expressed each of the combinations of the markers we examined (Figure 2L). In dCA2, 98.0% ± 1.3% of cells that expressed one of these prototypical markers co-expressed the two other CA2 markers examined (tdTomato, PCP4, and either RGS14 or STEP). In vCA2, PCP4 was the most widely expressed marker, present in 60% of DAPI-positive cells. Moreover, PCP4 was expressed in the majority of cells that co-expressed one or more of the three other CA2 markers (98%). Furthermore, in 36.1% ± 6.3% of PNs in the vCA2 region, PCP4 was the only CA2 marker these neurons expressed. In contrast, in dCA2 there were few if any cells that only expressed PCP4. The PCP4-only vCA2 cells appeared to be primarily in the deep pyramidal cell layer (cells located closer to stratum oriens). Nearly all PCP4-positive cells in vCA2 were excitatory (98.6%), based on co-expression of CaMKII (Figure S6). Moreover, the majority of CaMKII neurons in vCA2 expressed PCP4 (72.7%). Thus, the majority of vCA2 excitatory neurons expressed PCP4, while a significantly smaller fraction co-expressed tdTomato and RGS14/STEP (Figure S3). Altogether, these data reveal that PNs expressing dCA2 markers extend throughout the ventral region of the hippocampus, furthering previous results.[36]

Electrophysiological and anatomical properties of vCA2 PNs resemble those of dCA2

Given the difference in molecular heterogeneity we observed between dCA2 and vCA2 neurons, we performed whole-cell patch clamp recordings from vCA2 PNs to compare their electrophysiological properties with dCA2 neurons. vCA2 PNs had very similar intrinsic electrophysiological properties to those of dCA2 obtained in prior studies from our laboratory.[28] Thus, vCA2 and dCA2 PNs exhibited similar input resistance, membrane capacitance, and amplitude of voltage sag during membrane hyperpolarization, a hallmark of the hyperpolarization-activated cation current I_h (Figure S7). Of further note, the

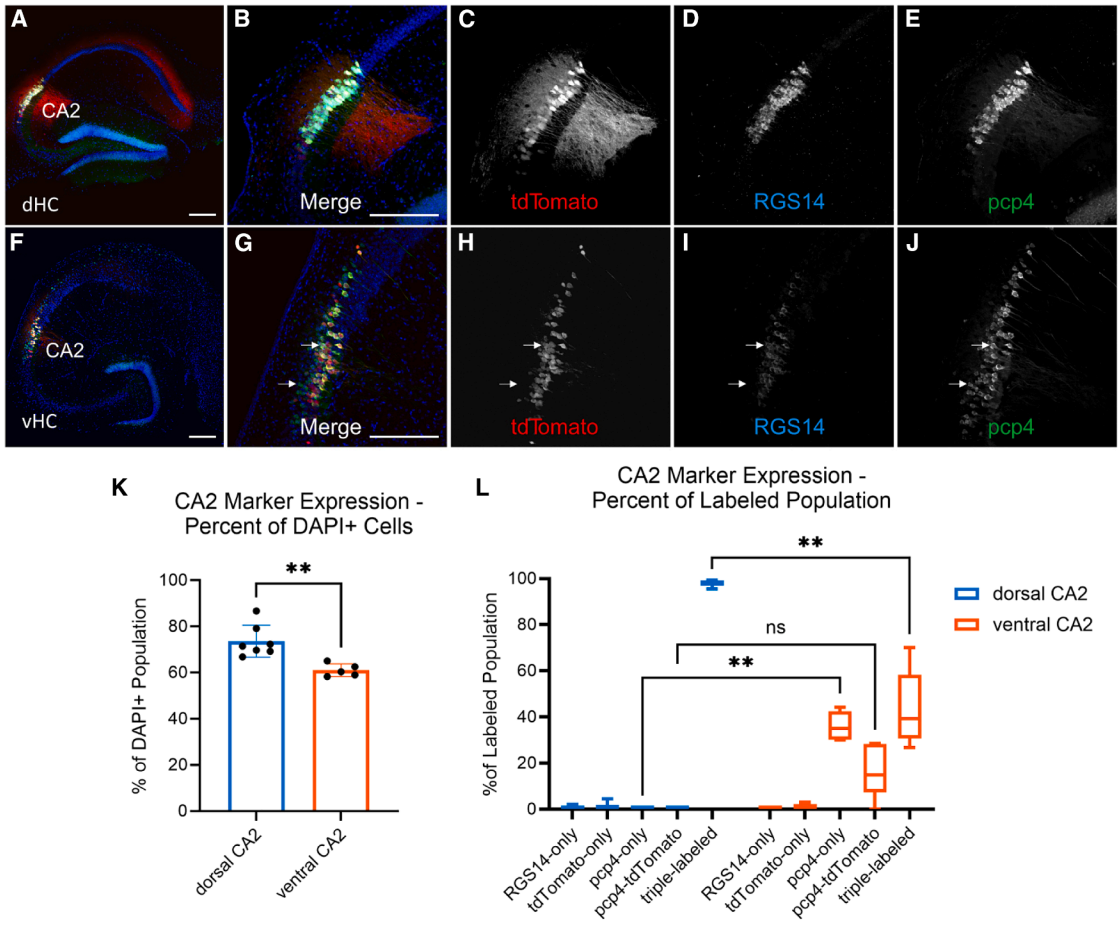

Figure 2. Distinct patterns of co-expression of prototypical CA2 markers and *Avpr1b*-Cre mediated expression in dorsal compared with ventral hippocampus

(A–E) Dorsal hippocampal transverse slices from *Avpr1b*-Cre$^{+/-}$ × Ai14 mice labeled with RGS14 (mouse $n = 3$) or STEP (mouse $n = 4$), co-labeled with PCP4 and DAPI.

(F–J) Ventral hippocampal transverse slices from *Avpr1b*-Cre$^{+/-}$ × *Ai14* mice labeled with RGS14 (mouse $n = 3$) or STEP (mouse $n = 2$), co-labeled with PCP4 and DAPI. Top white arrow indicates an example cell expressing two markers plus tdTomato (triple-labeled). Scale bar in A, B, F, and G, 200 μm. Bottom white arrow indicates an example cell that expressed PCP4 but not tdTomato (Avpr1b) or RGS14.

(K) Percentage of cells that expressed one or more of the three CA2 markers was significantly less in the vCA2 region than in the dCA2 region. Mann-Whitney test, $p = 0.0025$. Data represented as mean ± SEM.

(L) Percentage of cells that expressed the indicated combination CA2 marker(s) relative to the total subpopulation of cells in the vCA2 region that expressed at least one CA2 marker (PCP4, tdTomato/Avpr1b, and/or RGS14/STEP). In the dCA2 region, 98.0% ± 1.3% of cells expressed all three prototypical CA2 markers; none expressed only PCP4 (0.0% ± 0.0%). Significantly fewer cells expressed three markers (43.4% ± 16.5%) in vCA2 than dCA2 (note greater variance); significantly more vCA2 cells expressed only PCP4 (36.1% ± 6.3%) compared with dCA2 (two-way ANOVA Marker × Region, $F(4,44) = 79.51$, $p < 0.0001$). Šídák's multiple comparisons test for dCA2 vs. vCA2; RGS14 only, $p = 0.99$; tdTomato only, $p > 0.99$; PCP4 only, $p = 0.0011$; PCP4 and tdTomato, $p = 0.15$; triple-labeled, $p = 0.0087$). Central line is the median. Outer limits of box represent first and third quartiles. Whiskers represent max and min. ns = not significant, $^{**}p < 0.01$.

electrophysiological properties of vCA2 neurons were clearly distinct from those we recorded from ventral CA1 (vCA1) (Figure S7). Thus, neurons in vCA2 had a lower voltage sag in response to a hyperpolarizing current step, indicating a lower I_h, a lower input resistance, a higher rheobase, and a higher membrane capacitance compared with vCA1, very similar to the distinction between dCA1 and dCA2.[28] Notably, we did not observe any differences in electrophysiological properties in the subpopulations of Avpr1b-positive, Avpr1b-negative, and PCP4-negative vCA2 neurons based on post hoc immunohistochemical staining of biocytin-filled neurons (Figures S7G–S7I).

Dorsal CA2 and dCA1 PNs also differ in relative synaptic responses to their two major excitatory inputs: the direct perforant path inputs from entorhinal cortex, which target distal apical dendrites in stratum lacunosum moleculare (SLM), and the Schaffer collateral inputs from CA3 neurons, which target the more proximal apical dendrites in stratum radiatum (SR). Whereas the depolarizing postsynaptic potential (PSP) evoked by the direct EC inputs is much greater than that evoked by the Schaffer collateral inputs in dCA2, the inverse is found for dCA1.[28] To examine the synaptic responses of vCA2 neurons, we performed whole-cell recordings from transverse ventral

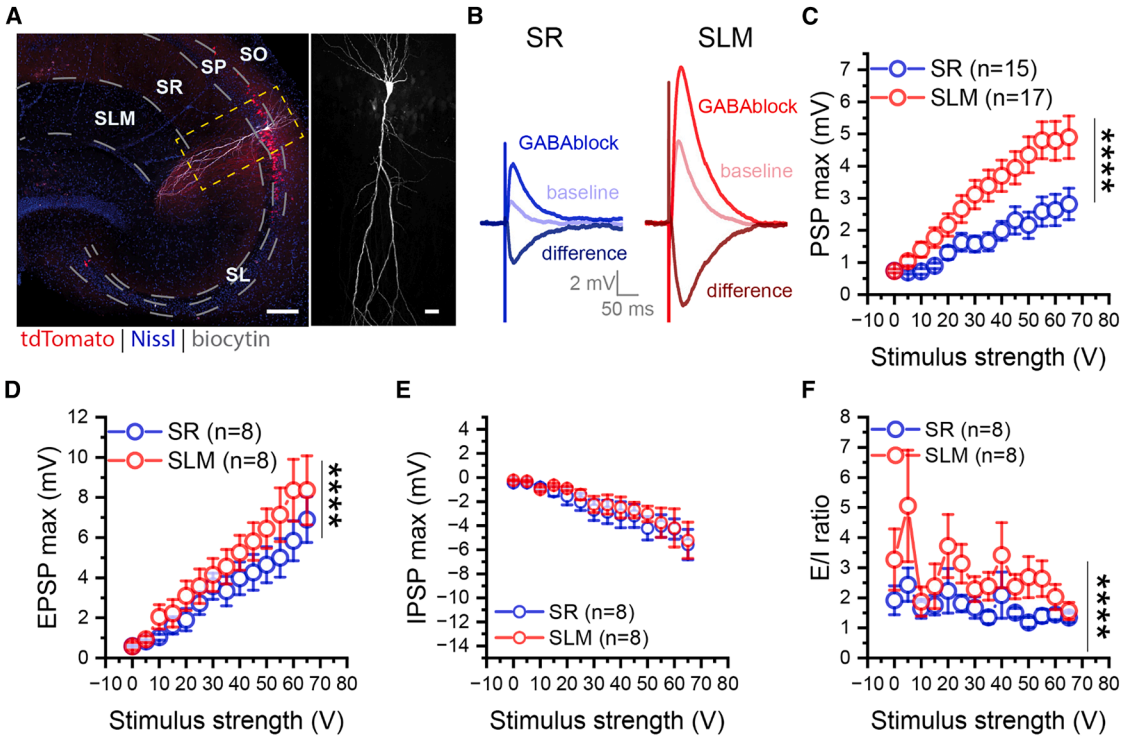

Figure 3. vCA2 PNs receive stronger excitatory inputs from EC than from CA3

(A) A transverse ventral hippocampal slice with a single biocytin-filled CA2 PN (white) from an *Avpr1b*-Cre$^{+/-}$ × *Ai14* mouse (left). Higher magnification view showing the morphological features of the same cell (right). Scale bars, 200 μm, left; 30 μm, right.

(B) Sample traces of compound PSPs (baseline), EPSPs recorded after applying GABA antagonists (GABAblock), and inferred IPSPs obtained by subtracting EPSP from baseline PSP (difference). EPSPs elicited with stimulating electrodes placed in SR to stimulate CA3 inputs (blue traces) or SLM to stimulate EC inputs (red traces).

(C and D) The amplitude of the PSP (C) and EPSP (D) evoked from SLM (red) was significantly larger than that evoked from CA3 (blue). PSP: two-way ANOVA $F(1,420) = 81.04$, $p < 0.0001$, SR: $n_{mice} = 9$, SLM: $n_{mice} = 10$. EPSP: two-way ANOVA $F(1,196) = 16.73$, $p < 0.0001$, SR: $n_{mice} = 5$, SLM: $n_{mice} = 6$.

(E) IPSPs evoked from SLM and SR were similar in amplitude. Two-way ANOVA $F(1,196) = 1.973$, $p = 0.1617$. SR, $n = 5$ mice; SLM, $n = 6$ mice.

(F) The EPSP/IPSP amplitude ratio evoked from SLM was greater than that from SR. Two-way ANOVA, $F(1,196) = 19.09$, $p < 0.0001$. SR, $n = 5$ mice, SLM, $n = 6$ mice. ****$p < 0.0001$. Data are represented as mean ± SEM.

hippocampal slices from *Avpr1b-Cre*$^{+/-}$ × *Ai14* reporter mice, targeting the CA2 region of the slice based on tdTomato fluorescence (although we did not target specifically the tdTomato-positive neurons), while activating inputs with a stimulating electrode in SLM or SR (Figure 3).

Similar to results in dCA2,[28] vCA2 PNs generated a much larger depolarizing PSP in response to stimulation in SLM compared with SR (Figures 3B and 3C). As the PSP is the net voltage response generated by the excitatory glutamatergic postsynaptic potential (EPSP) and the inhibitory GABAergic postsynaptic potential (IPSP), we examined the EPSP by blocking the IPSP with antagonists of $GABA_A$ receptors (SR-95531) and $GABA_B$ receptors (CGP-35348). Previous recordings from dCA2 found that whereas the amplitudes of the SLM and SR EPSPs are similar in amplitude, SR stimulation elicits a stronger feedforward inhibition compared with SLM. As a result, the EPSP/IPSP ratio and peak net PSP depolarization is greater with SLM compared to SR stimulation.[28] In contrast to results in dCA2, the EPSP elicited by SLM stimulation in vCA2 was significantly greater than that elicited by SR stimulation (Figures 3B and 3D), whereas the inferred IPSPs (obtained by subtracting the EPSP from the PSP) were similar (Figures 3B and 3E). As a result the EPSP to IPSP ratio was greater with SLM stimulation compared with SR stimulation in both dorsal[28] and ventral CA2 (Figure 3F), although for different underlying reasons.

Next, we examined the morphological properties of vCA2 PNs by performing patch clamp recordings with biocytin in the pipette solution in *Avpr1b-Cre*$^{+/-}$ × *Ai14* mice. Similar to the neuronal morphology in dCA2,[28,39,40] the apical dendrites of vCA2 PNs bifurcated closer to the soma (62.28 ± 10.33 μm, $n = 25$) than did vCA1 apical dendrites (186.9 ± 17.53 μm, $n = 29$; vCA2 vs. vCA1: $t = 6.128$, $p < 0.0001$). Lorenté de Nò distinguished CA2 neurons from CA3 neurons based on the absence or presence, respectively, of large dendritic spines (thorny excrescences) in stratum lucidum (SL), the site of the mossy fiber synapses from dentate gyrus granule cells.[1] We found that whereas vCA3 PNs had characteristically large spines in SL (Figure S9), tdTomato-positive vCA2 PNs lacked detectable thorny excrescences, similar to the vast majority (if not all[37]) dCA2 PNs (Figure S8).

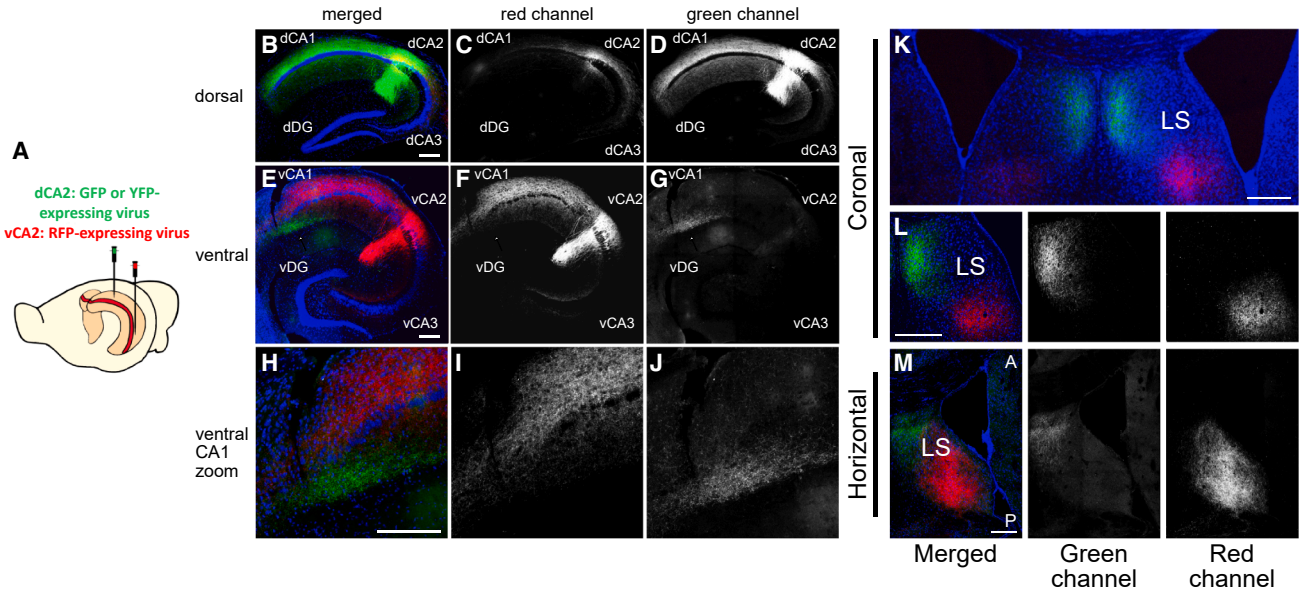

Figure 4. Dual fluorescent protein expression in dCA2 and vCA2 reveals a topographic projection pattern along the hippocampal dorso-ventral axis and in lateral septum

(A) Experimental scheme. Cre-dependent GFP- or YFP-expressing AAV injected in dCA2 and Cre-dependent RFP-expressing AAV injected in vCA2 in *Avpr1b*-Cre$^{+/-}$ mouse.

(B–J) Transverse slices from dorsal hippocampus (B–D) and ventral hippocampus (E–J). Scale bar in B, E, and H, 200 μm. (B and E) Composite tiled images of injection site in dCA2 (B) and vCA2 (E). (C and F) Red channel, vCA2 projections to dorsal (C) and ventral (F) hippocampus. Green channel, dCA2 projections to dorsal (D) and ventral (G) hippocampus. (H) Zoomed image of vCA1 from composite image in (E) showing distinct projection pattern of dCA2 and vCA2 to vCA1. (I) vCA2 projection to vCA1 (red channel) was predominantly located in stratum orients. (J) dCA2 projection to vCA1 (green channel) was predominantly located in stratum radiatum. Scale bar, 200 μm. White arrow indicates magnified vCA1 region in (H)–(J).

(K) 5x composite image of a coronal slice from an *Avpr1b*-Cre$^{+/-}$ mouse injected with Cre-dependent AAV to express EYFP in dCA2 and mCherry in vCA2. Images show projections from dCA2 (green) to anterior dorsal lateral septum and from vCA2 (red) to posterior ventral lateral septum. Scale bar in K, 200 μm.

(L) Left: 20x merged image of projections from dCA2 (green) and vCA2 (red) to lateral septum. Center: dCA2 projections only (green channel). Right: vCA2 projections only (red channel). Scale bar in L (left), 200 μm.

(M) Left: 10x horizontal tile from *Avpr1b*-Cre$^{+/-}$ mouse showing projections from dCA2 (green) to anterior dorsal lateral septum and projections from vCA2 (red) to posterior ventral lateral septum. White A indicates anterior side; white P indicates posterior side. Center: dCA2 projections only (green channel). Right: vCA2 projections only (red channel). Scale bar in M (left), 200 μm.

vCA2 PNs project to distinct areas within vCA1 and lateral septum compared with dCA2

Next, we examined whether dorsal and ventral CA2 neurons projected to similar or distinct brain regions. Dorsal CA2 sends dense projections to dCA1 and dorsal lateral septum, as well as somewhat weaker projections to vCA1. Outputs from dCA2 to dorsal lateral septum promote social aggression,[22] while outputs from dCA2 to vCA1 enable social memory.[17] To date, the outputs of genetically identified vCA2 neurons remain unknown.

To compare dCA2 and vCA2 projections, we performed anterograde tracing by injecting *Avpr1b-Cre*$^{+/-}$ mice with Cre-dependent AAV expressing GFP or YFP in dCA2 (n = 4) and RFP in vCA2 (n = 4).

We observed a topographic pattern of intrahippocampal projections along the CA2 dorsoventral axis (Figure 4), with dCA2 projecting most strongly to dCA1 and vCA2 projecting strongly to vCA1. Interestingly, vCA2 sent its densest projections to vCA1c (near the border with vCA2) and vCA1b (middle of vCA1), complementary to the vCA1a region targeted by dCA2 (near the border with subiculum). The projections from dCA2 and vCA2 to vCA1 also targeted complementary radial layers of vCA1, with dCA2 axons largely confined to SR and vCA2 axons largely confined to stratum oriens, the same region with densest projections from dCA2 to dCA1[17] (Figures 4G and 4J).

Similar to dCA2, the primary extrahippocampal output from vCA2 targeted the lateral septum. As described for other hippocampal inputs to lateral septum,[41] the CA2 projection was topographic, with dCA2 projecting to dorsal anterior lateral septum and vCA2 projecting to more ventral posterior lateral septum, as previously described using non-genetic-based tracer approaches[36] (Figures 4K–4M).

Next, we performed electrophysiological recordings to determine the synaptic strength of the vCA2 outputs to vCA1. We injected *Avpr1b-Cre*$^{+/-}$ animals with Cre-dependent AAV to express ChR2 in vCA2 PNs and compared the optogenetically evoked postsynaptic potentials recorded in vCA1a with the responses recorded in vCA1b/c (Figure 5). In agreement with the anatomical projection data, photostimulation of vCA2 axons evoked a measurable postsynaptic depolarization in a significantly greater fraction of vCA1b/c PNs compared with vCA1a (Figure 5B; chi-square, z = 2.338, p = 0.019), with a mean peak depolarization and positive voltage-time integral significantly

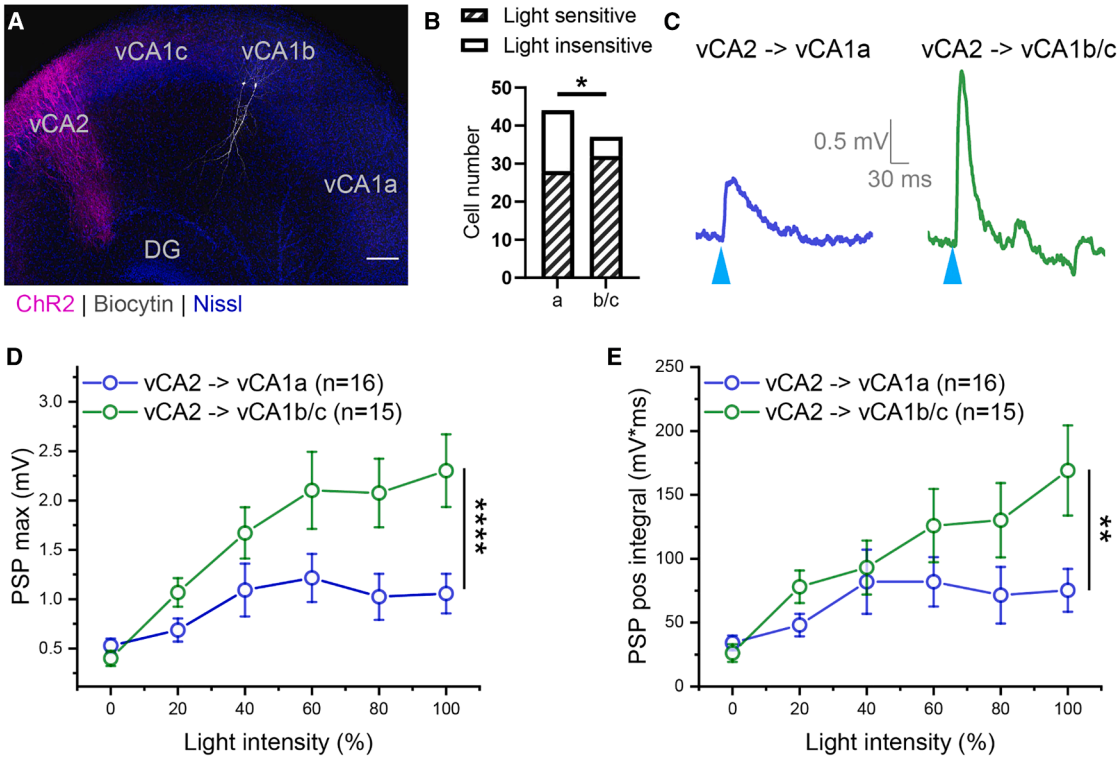

Figure 5. Optogenetic activation of vCA2 evokes larger PSP in PNs in vCA1b/c compared with vCA1a

(A) *Avpr1b*-Cre$^{+/-}$ mice were injected with Cre-dependent AAV to express ChR2 in vCA2. Light-evoked PSPs or postsynaptic currents were measured, respectively, in current-clamped or voltage-clamped PNs in vCA1a or vCA1b/c. Membrane held at −70 mV. White neurons in vCA1b show biocytin staining following patch clamp recordings with biocytin in electrode. Scale bar, 100 μm.

(B) Proportion of neurons in vCA1a and vCA1b/c with measurable light-evoked synaptic responses (chi-square, $z = 2.338$, $p = 0.019$). Cells recorded from voltage clamp and current clamp were pooled.

(C) Example traces of light-evoked PSP in PNs in vCA1a and vCA1b/c.

(D) Peak current-clamped PSP amplitude as a function of light intensity recorded in vCA1a and vCA1b/c PNs. PSP was significantly larger in vCA1b/c compared with vCA1a. Two-way ANOVA, vCA1a vs. vCA1b/c: $F(1, 174) = 21.99$, $p < 0.0001$.

(E) Integral of light-evoked PSP was significantly larger in vCA1b/c compared with vCA1a. Two-way ANOVA, vCA1a vs. vCA1b/c: $F(1,174) = 9.833$, $p = 0.002$). $^{**}p < 0.01$, $^{****}p < 0.0001$. Data are represented as mean ± SEM.

larger in vCA1b/c compared with vCA1a (Figures 5D and 5E, two-way ANOVA vCA1a vs. vCA1b/c; PSP max: $F(1,174) = 21.99$, $p < 0.0001$; PSP positive integral: $F(1,174) = 9.833$, $p = 0.002$). These results are complementary to the previous finding that dCA2 elicits a reliable depolarization in vCA1a neurons but not in vCA1b/c neurons.[17]

We next performed voltage-clamp recordings to measure the vCA1 excitatory and inhibitory postsynaptic currents (EPSCs and IPSCs) elicited by optogenetic activation of vCA2. For comparison, we also measured the EPSCs and IPSCs from dCA1 neurons in response to optogenetic activation of dCA2. Optogenetic activation of dCA2 and vCA2 produced similar-sized peak EPSCs in dCA1 and vCA1, respectively, with no significant difference (Figure S10A). In contrast to findings that dCA2 elicits a larger EPSC in deep compared with superficial dCA1 PNs,[42] we found no difference between deep and superficial layer vCA1 EPSCs in response to vCA2 activation ($p = 0.327$; Kolmogorov-Smirnov test). As a further contrast, optogenetic activation of vCA2 elicited a significantly larger IPSC in vCA1 neurons compared with the IPSC recorded in dCA1 in response to optogenetic activation of dCA2 (Figure S10B). As a result, the IPSC/EPSC ratio was significantly larger in vCA1 compared with dCA1 (Figure S10D).

The above results indicate that Avpr1b-expressing cells in the ventral hippocampus exhibited many of the morphological, molecular, electrophysiological, and synaptic properties of dCA2 neurons. However, there was greater molecular heterogeneity in neurons in the anatomic vCA2 region compared with its dorsal counterpart. Moreover, dorsal and ventral CA2 neurons projected to complementary topographic regions in lateral septum and subregions along the transverse axis of vCA1.

Avpr1b-expressing cells in vCA2 are not necessary for social memory

Given the well-defined role of dCA2 in SNRM, we next examined whether vCA2 played a similar behavioral role (Figure 6). We used a chemogenetic approach, similar to that used to study dCA2,[17] by injecting a Cre-dependent AAV in either dCA2 (Figure 6B) or vCA2 (Figure 6E) of *Avpr1b-Cre*$^{+/-}$ mice to express the hM4Di inhibitory designer receptor exclusively activated by

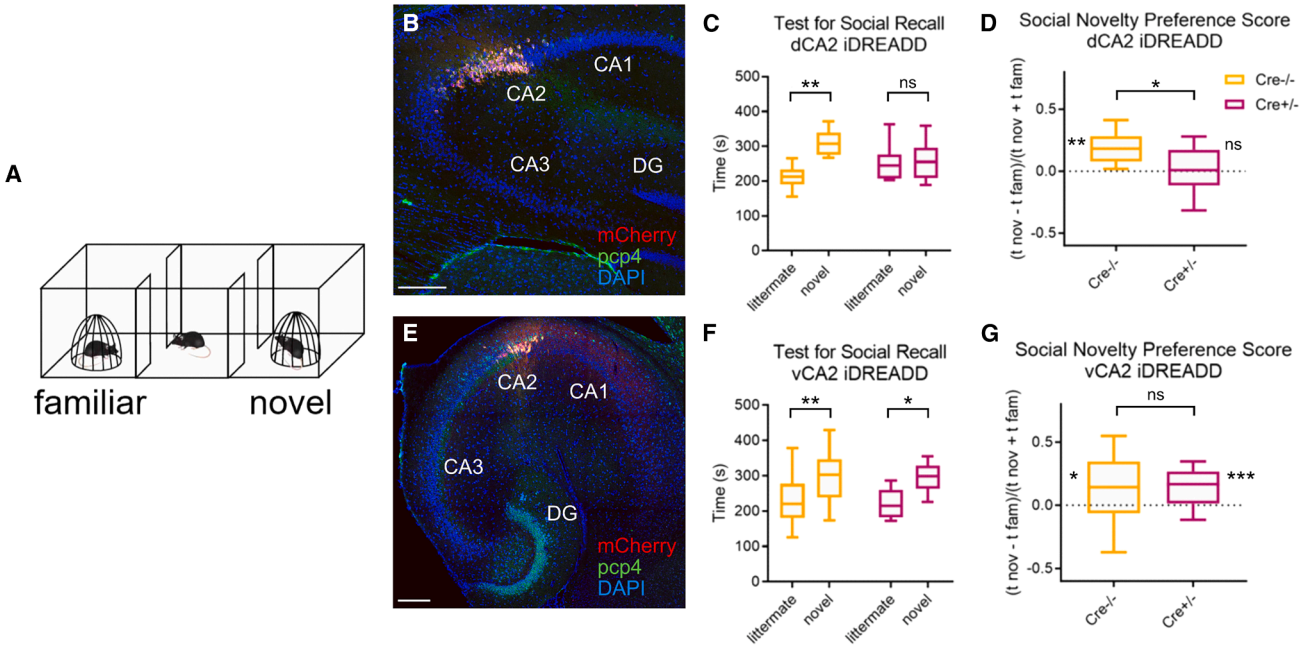

Figure 6. Pharmacogenetic inhibition of Cre-expressing cells in dCA2 but not vCA2 of *Avpr1b-Cre*$^{+/-}$ mice blocks social memory recall

Avpr1b-Cre$^{+/-}$ (data shown in magenta) and Cre$^{-/-}$ (data shown in orange) littermates injected in either dCA2 (B–D) or vCA2 (E–G) with Cre-dependent mCherry-iDREADD AAV.

(A) One-trial test for social memory recall. A subject mouse explored a three-chamber arena with a familiar littermate and novel conspecific confined under wire pencil cup cages in opposite chambers for 10 min.

(B) Dorsal hippocampal transverse slice co-stained for mCherry and PCP4. Scale bar, 200 μm.

(C) Exploration times of littermate and novel mouse in social memory test for *Avpr1b-Cre*$^{+/-}$ (n = 16) and *Cre*$^{-/-}$ (n = 16) littermates. Both groups administered CNO 30 min prior to test. *Cre*$^{-/-}$ but not *Cre*$^{+/-}$ littermates injected in dCA2 preferentially explored the novel mouse. Two-way ANOVA genotype × interaction partner F(1,30) = 6.937, p = 0.013; Šídák's multiple comparisons test: Cre$^{-/-}$, littermate vs. novel, p = 0.0003; Cre$^{+/-}$, littermate vs. novel, p = 0.76.

(D) Discrimination Index measure of preference for novel vs. familiar mice was significantly different from zero for *Cre*$^{-/-}$ but not *Cre*$^{+/-}$ mice. One-sample t test against zero: Cre$^{-/-}$, t = 5.306, df = 15, p < 0.0001; Cre$^{+/-}$, t = 0.5603, df = 15, p = 0.56. Unpaired t test between Cre$^{-/-}$ and Cre$^{+/-}$ mice, t = 2.687, df = 30, p = 0.012.

(E) ventral hippocampal transverse slice co-stained for mCherry and PCP4.

(F) Both Cre$^{-/-}$ (n = 24) and Cre$^{+/-}$ mice (n = 18) injected in vCA2 interact more with novel compared with familiar littermate. Two-way ANOVA interaction partner F(1,40) = 16.71, p = 0.0002; genotype × interaction partner, F(1,40) = 0.005, p = 0.94; followed by Šídák's multiple comparisons test for littermate vs. novel: Cre$^{-/-}$, p = 0.0078; Cre$^{+/-}$, p = 0.018. A greater interaction time with the novel over familiar littermate is only observed in Cre$^{+/-}$ mice expressing iDREADD in vCA2 compared with dCA2 (two-way ANOVA interaction partner × brain region F(1,32) = 4.938, p = 0.0335; followed by Šídák's multiple comparisons test for littermate vs. novel: dCA2, p = 0.80; vCA2, p = 0.010).

(G) Discrimination index for Cre$^{-/-}$ and Cre$^{+/-}$ mice was significantly greater than zero. One-sample t test against zero: Cre$^{-/-}$, t = 2.648, df = 23, p = 0.014; Cre$^{+/-}$, t = 3.988, df = 17, p = 0.001. Unpaired t test comparing Cre$^{-/-}$ and Cre$^{+/-}$, t = 0.1545, df = 40, p = 0.88. There was a significant difference between discrimination index of Cre$^{+/-}$ mice injected with Cre-dependent mCherry-iDREADD in dCA2 (data from D) vs. vCA2 (G). Unpaired t test t = 2.265, df = 32, p = 0.030. Central line is the median. Outer limits of box represent first and third quartile. Whiskers represent max and min. *p < 0.05,**p < 0.01, ***p < 0.001, ns = non-significant.

designer drugs (iDREADD). *Cre*$^{-/-}$ littermate controls were injected in either dCA2 or vCA2 with the same AAV.

We first compared the effect of silencing dCA2 and vCA2 in a one-trial social novelty recognition task. Three weeks following AAV injection, mice were tested for their ability to discriminate a littermate from a novel mouse (Figure 6). Both groups were injected intraperitoneally with the DREADD ligand clozapine-N-oxide (CNO; 10 mg/kg) 30 min prior to testing. Subjects were first habituated to a three-chamber arena containing empty wire cup cages in the end chambers of the arena. We then placed a familiar littermate and novel conspecific under each of the wire cups and allowed the subjects to explore the mice in the arena for 10 min. Social novelty preference was assessed by the normal preference of a subject to explore the novel individual compared with the familiar littermate. We quantified the absolute interaction times and calculated a behavioral discrimination score, defined as the time spent exploring the novel mouse minus the time spent exploring the littermate divided by the total interaction time with both individuals.

As previously described for *Amigo2*-Cre mice,[14,17] silencing dCA2 in *Avpr1b-Cre*$^{+/-}$ mice suppressed the normal preference of the subject to explore the novel compared with familiar mouse. Thus, whereas *Cre*$^{-/-}$ control mice spent a significantly greater time investigating the novel individual compared with the familiar littermate (Figure 6C), with a discrimination index significantly greater than zero (Figure 6D), *Avpr1b-Cre*$^{+/-}$ mice failed

to distinguish the novel mouse from the familiar littermate. These results thus confirm that dCA2 is crucial for SNRM in distinct mouse lines. In contrast, silencing vCA2 in *Avpr1b-Cre*$^{+/-}$ mice expressing iDREADD failed to suppress SNRM. Thus, both *Avpr1b-Cre*$^{+/-}$ and *Cre*$^{-/-}$ control mice spent a significantly greater time interacting with the novel compared with the familiar animal, with a discrimination index significantly greater than zero in both groups. Moreover, there was no significant difference in interaction times or discrimination index between the two groups of mice (Figures 6F and 6G).

A comparison of the interaction times in *Avpr1b-Cre*$^{+/-}$ dCA2-silenced and vCA2-silenced mice (Figures 6C and 6F) showed that the latter group spent a significantly greater time exploring the novel compared with familiar mice than did the dCA2-silenced group (see legend to Figure 6 for statistics). In addition, the discrimination index was significantly greater in vCA2-silenced (Figure 6G) compared with dCA2-silenced mice (Figure 6D; see legend to Figure 6 for statistics).

Similar to results with dCA2 silencing,[14,17] silencing vCA2 did not impair sociability, measured by total social exploration time in the social memory test (Figure S11) or preference for exploring a social compared with non-social stimulus (Figure S12). In addition and similar to dCA2 inhibition,[14] vCA2 inhibition did not alter exploration of non-social or social (urine) odors, nor did it impair habituation or dishabituation to social or non-social odors (Figure S13). Thus, in contrast to the importance of dCA2 for social memory, Cre-expressing vCA2 cells in *Avpr1b-Cre*$^{+/-}$ mice were not necessary for the discrimination of a novel individual from a familiar littermate.

As the ability of an animal to distinguish a novel from a familiar littermate primarily relies on recall of a highly consolidated memory, we next performed a two-trial social memory recognition task in which subjects must encode and consolidate a new memory of a novel individual (Figure S14A). In this task, a subject mouse first explored two novel individuals under wire cup cages in an open arena for 5 min; the subject was then returned to its home cage. After 30 min, the subject was returned to the arena for a 5-min recall trial in which one of the two subjects from the first trial was replaced by a previously unencountered novel individual. SNRM was assessed by the preferential exploration of the novel individual compared with the now familiarized individual encountered in the learning trial.

Previous studies have shown that silencing dCA2 with chemogenetics or optogenetics during the learning trial prevents the discrimination of the novel and familiarized mouse in the recall trial.[17,18] In contrast, we found that systemic injection of CNO 30 min prior to the social memory test in *Avpr1b-Cre*$^{+/-}$ mice expressing hM4Di in vCA2 failed to inhibit social memory. Thus, both *Avpr1b-Cre*$^{+/-}$ mice and *Cre*$^{-/-}$ littermate controls (also injected with CNO) spent significantly more time interacting with the novel individual compared with the familiar one (Figure S14B), with discrimination indexes significantly greater than zero (Figure S14C). Again, no difference was observed between groups (two-way repeated measures ANOVA Genotype × Interaction Partner $F(1,38) = 0.6985$, $p = 0.70$; unpaired t test $t = 0.1270$, $df = 38$, $p = 0.90$).

Because Cre was expressed in the *Avpr1b-Cre*$^{+/-}$ mice in a smaller fraction of vCA2 neurons (38.0% ± 5.4%) compared with dCA2 neurons (72.4% ± 8.8%), the lack of effect of silencing vCA2 on social memory could be due to the lower proportion of total cells in vCA2 that were inhibited with this line. As we found that PCP4 was expressed in a wider fraction of neurons compared with *Avpr1b*-Cre-mediated expression (60% of all cells within the vCA2 region compared with 38%), we next determined the efficacy of chemogenetic silencing of vCA2 on social memory using a *PCP4-Cre*$^{+/-}$ mouse line.[43]

As this line had not been previously used to target CA2, we first examined the efficacy and specificity of *PCP4-Cre*-mediated targeting of vCA2 (Figures S15A and S15B). We found that injection of a Cre-dependent AAV in vCA2 of *PCP4-Cre*$^{+/-}$ mice led to widespread and relatively selective expression in vCA2 (Figure S15A). However, as PCP4 is also expressed in dentate gyrus, extra care was taken with the targeting of viral injection to limit expression to CA2. Quantitatively, 53.9% ± 2.3% ($n = 16$) of DAPI-expressing vCA2 cells expressed a Cre-dependent AAV marker, close to the 60% of vCA2 cells that express PCP4.

Chemogenetic silencing the broader population of PCP4-expressing vCA2 neurons also failed to inhibit social memory recall in the one-trial (littermate vs. novel mouse) social memory test (Figures S15C and S15D). Thus, both *PCP4-Cre*$^{+/-}$ and *Cre*$^{-/-}$ littermates spent significantly more time exploring the novel individual compared with the familiar littermate, with no significant difference between groups (two-way repeated measures ANOVA, Genotype × Interaction Partner $F(1,17) = 0.7533$, $p = 0.75$ followed by Šídák's multiple comparisons test for exploration of littermate vs. novel mouse: *Cre*$^{-/-}$ controls, $p = 0.0024$; *PCP4-Cre*$^{+/-}$, $p = 0.0014$). Altogether these results suggest that vCA2 neurons are less critical for social memory compared with dCA2.

PCP4-expressing cells in vCA2 modulate social aggression

In addition to its role in social memory, dCA2 promotes social aggression[22,33] and this action is more pronounced during encounters with novel mice.[44] As ventral hippocampus has been implicated in behaviors tied to emotional states,[7,9,45,46] we hypothesized that vCA2 may play a more important role in regulating aggression than in social memory discrimination. We thus used the resident-intruder test to determine the effect of silencing vCA2 on aggression in *PCP4-Cre*$^{+/-}$ residents expressing iDREADD compared with *Cre*$^{-/-}$ controls (Figure 7). Three weeks following AAV injection in vCA2, we introduced a novel BALBc intruder into the cage of a singly housed resident for 5 min. We then repeated this test once a day over 3 successive days using the same BALBc intruder. On days 1–3, we injected both cohorts of residents with saline 30 min prior to testing aggression. On day 4, we examined the effect of silencing CA2 on aggression by injecting CNO systemically in both groups of mice prior to introducing a novel BALBc intruder for a 10-min resident-intruder test.[44] During the first 3 days of the testing (saline injection), *PCP4-Cre*$^{+/-}$ and Cre$^{-/-}$ residents displayed similar levels of aggression toward the BALBc intruder, as measured by the number of biting attacks and total attack duration, indicating that there was no effect of genotype on aggression (two-way repeated measures ANOVA, attack bouts: *PCP4-Cre*$^{+/-}$ vs. *Cre*$^{-/-}$ $F(1,4) = 1.089$, $p = 0.3555$; total attack duration: *PCP4-Cre*$^{+/-}$ vs. *Cre*$^{-/-}$

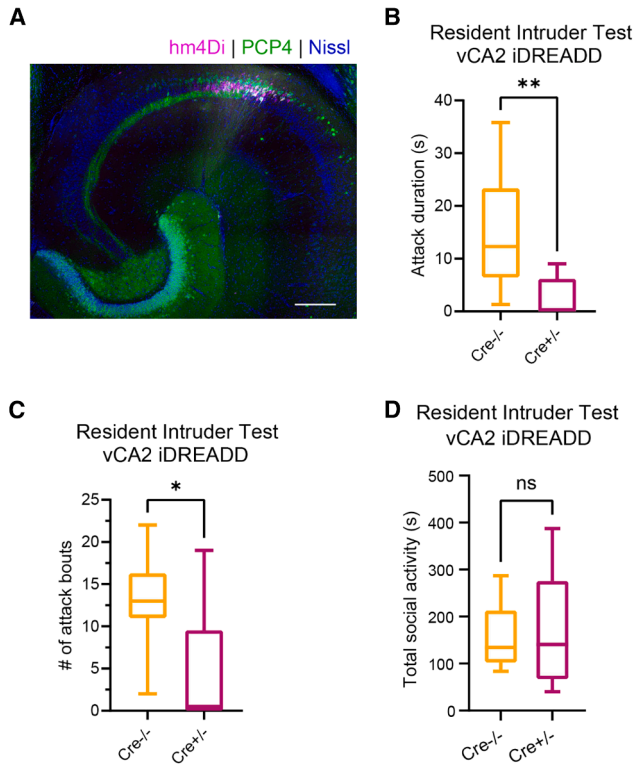

Figure 7. Inhibition of Cre-expressing neurons in vCA2 of *PCP4-Cre*$^{+/-}$ mice decreases social aggression

PCP4-*Cre*$^{+/-}$ (data shown in magenta) and Cre$^{-/-}$ (data shown in orange) littermates injected in vCA2 with Cre-dependent mCherry-iDREADD AAV.

(A) Ventral hippocampal transverse slice co-stained for mCherry and PCP4. Scale bar, 200 μm.

(B) Three weeks following viral injection, both groups of subjects (residents) were administered CNO 30 min prior to exposure to a novel mouse intruder in a resident-intruder test. Total time spent in attack was significantly lower in *Cre*$^{+/-}$ ($n = 8$) compared with *Cre*$^{-/-}$ ($n = 8$) residents. Median attack duration: *Cre*$^{-/-}$ = 12.3 s; *Cre*$^{+/-}$ = 0.15 s; Mann-Whitney test, $p = 0.0042$.

(C) *Cre*$^{-/-}$ residents showed significantly more attack bouts compared with *Cre*$^{+/-}$ residents (median *Cre*$^{-/-}$ = 13 attacks, median *Cre*$^{+/-}$ = 0.5 attacks, Mann-Whitney test, $p = 0.018$).

(D) *Cre*$^{+/-}$ and *Cre*$^{-/-}$ subjects displayed similar total duration of all social interactions (total = time spent in aggression + social dominance + social investigation). Median *Cre*$^{-/-}$ = 134.3 s, median *Cre*$^{+/-}$ = 140.6 s, Mann-Whitney test, $p = 0.8517$. Central line is the median. Outer limits of box represent first and third quartile. Whiskers represent max and min. $^{**}p < 0.01$, $^{*}p < 0.05$, ns = non-significant.

$F(1,4) = 0.8616$, $p = 0.4058$). In contrast, injection of CNO during the fourth day led to a large decrease in aggression toward the novel BALBc intruder in the iDREADD-expressing mice relative to the *Cre*$^{-/-}$ control group (Figures 7B and 7C). CA2 silencing caused a significant decrease in both the total duration of aggression (median = 12.3 s for *Cre*$^{-/-}$ compared with 0.15 s for *PCP4-Cre*$^{+/-}$ groups; Mann-Whitney test, $p = 0.0042$) and the number of bouts of aggression (median = 13 for *Cre*$^{-/-}$ compared with 0.5 for *PCP4-Cre*$^{+/-}$ groups; Mann-Whitney test, $p = 0.018$). The decrease in aggression was not associated with a loss of social interest as there was no difference in the total duration of all social interactions in the two groups (Figure 7D).

DISCUSSION

Here, we provide, to our knowledge, the first comprehensive analysis of the molecular, morphological, and electrophysiological properties of vCA2 PNs and the first examination of their behavioral role. Our results support the existence of a population of PNs in the anatomically defined CA2 region of the ventral hippocampus that share key molecular markers, cellular morphology, and electrophysiological and synaptic properties with the well-defined population of CA2 neurons in dorsal hippocampus. However, we find a greater molecular heterogeneity in vCA2 compared with dCA2 PNs, as well as both shared and distinct behavioral roles.

The differences and similarities in the behavioral roles of ventral compared with dorsal CA2 may be explained by the differences and similarities in the synaptic targets of these two regions. Our laboratory previously found that dCA2 regulates SNRM through its projections to the stratum radiatum region of vCA1a, the vCA1 region bordering the subiculum.[17] In contrast, here we found that vCA2 preferentially targets the stratum oriens of a complementary region of vCA1, vCA1b and vCA1c, which lie more proximal to vCA2 (Figure 4). These anatomical results are consistent with our electrophysiological results in which optogenetic activation of dCA2 inputs to ventral CA1 elicit a stronger excitatory response in vCA1a compared with vCA1b/c.[17] In contrast, we found that optogenetic activation of vCA2 produced much stronger synaptic excitation of vCA1b,c compared with vCA1a (Figure 5). Thus, the differential roles of dCA2 and vCA2 in SNRM may be a result of this different pattern of synaptic targeting within vCA1.

A second possible reason why vCA2 PNs do not promote SNRM is that their projections to vCA1 elicit a larger feedforward inhibition than that elicited by dCA2 to dCA1 (Figure S10). Thus, activation of dCA2 produced a significantly smaller IPSC in neurons in dCA1 compared with the IPSC evoked in vCA1 in response to activation of its vCA2 inputs. Thus, vCA2 may dampen, rather than excite, vCA1a neuron activity, in opposition to the excitatory action of dCA2, providing a potential explanation as to why vCA2 silencing does not inhibit SNRM. While we hypothesize that the differential projections to vCA1 are responsible for the differences we observe in function, it is important to note that other inputs to CA2 that have been implicated in social memory, such as the supramammillary nucleus,[47,48] medial septum,[19] and entorhinal cortex,[13] may be responsible for the differential roles of dorsal and ventral CA2 on social memory.

In contrast to their differential roles in regulating social memory, vCA2 and dCA2 exert similar actions to promote social aggression. Of particular interest, both regions appear necessary to mount an aggressive response, as inhibition of either region alone is sufficient to almost fully suppress aggression. Our laboratory previously found that dCA2 promoted aggression through its projections to inhibitory neurons in dorsal lateral septum. Activation of these neurons by dCA2 resulted in the disynaptic inhibition of neurons in ventral lateral septum that tonically suppress aggression through their outputs to VMHvl of the hypothalamus.[22] In this manner, an increase in dCA2 activity acted to disinhibit aggression. While we have not identified the circuit by which vCA2 promotes social aggression, we hypothesize it requires the vCA2

output to lateral septum. Although vCA2 targets a region of lateral septum that is more ventral than that targeted by dCA2, both projection zones fall within the confines of classically defined dorsal lateral septum.[41] It is thus likely that the vCA2 projections to lateral septum also promote aggression by inhibiting neurons in ventral lateral septum, thereby disinhibiting VMHvl. As the silencing of either dCA2 or vCA2 is sufficient to suppress aggression, the two sets of lateral septum neurons activated by dCA2 and vCA2 may converge on a common population of ventral lateral septum neurons, acting synergistically to inhibit these neurons, thereby disinhibiting VMHvl.

Previous studies have also demonstrated the importance of Avpr1b, which is highly enriched in CA2 PNs compared with almost all other regions of the brain, in promoting both social aggression[22,32,33] and social memory behavior.[16] Pagani et al.[33] found that social aggression could be partially rescued in a general Avpr1b knockout by lentiviral-mediated expression of Avpr1b targeted mainly to dorsal CA2. Of interest, although viral expression of Avpr1b in dCA2 restored to normal levels the percentage of mice that attacked an intruder, attack latency was only partially rescued. This incomplete rescue could be explained if Avpr1b expression in vCA2 was necessary to achieve normal levels of aggression.

Altogether, our results provide evidence for the existence of a broadly defined category of CA2 PNs along the entire longitudinal axis of the hippocampus that share certain molecular, anatomical, and electrophysiological properties. Future work is needed to assess the nature of the social representations in vCA2 to determine whether they discriminate social novelty from familiarity as described in dCA2[49,50] or whether vCA2 selectively encodes behavioral state, reflecting its role in promoting aggression, Finally, if, as hypothesized, vCA2 modulates social aggression through its output to lateral septum, the purpose of its prominent projections within the hippocampus to vCA1b and vCA1c remains elusive.

Limitations of the study

In this work, we have employed two mouse models that allow specific access to cells within the ventral CA2 region (Avpr1b and PCP4). PCP4 has a broader expression profile compared with Avpr1b, in line with prior reports.[37] At this point, it is unclear if the excitatory cells in the region that are Avpr1b and/or PCP4 negative are distinct in their pattern of molecular expression from vCA1 or vCA3 PNs. In principle, the heterogeneity in marker expression in vCA2 could reflect the migration of molecularly defined vCA1 or vCA3 PNs into vCA2 territory. However, we found that neurons in vCA2, regardless of marker expression, have similar electrophysiological properties to each other that resemble the properties of dCA2 neurons. Moreover, these properties are clearly distinct from those of vCA1 neurons. Although we have not examined vCA3 electrophysiological properties in detail, these neurons are distinguishable from vCA2 neurons because the former are studded with thorny excrescences, which neurons in vCA2 lack. Thus, we think it unlikely that a substantial fraction of neurons in vCA2 could be misplaced vCA1 or vCA3 neurons.

A previous study found considerable heterogeneity in dendritic morphology of neurons in the dorsal CA2 region.[40] We also see heterogeneity in terms of apical dendritic length based on staining of neurons filled with biocytin during patch clamp recordings. However, because we did not target neurons deep within the slice, we cannot rule out the possibility that some of the heterogeneity in dendritic length may have resulted from severing of the dendrites during patch clamp recordings. Thus, future careful examination of this question is required. A limitation with our behavioral findings on social memory is that PCP4 is not expressed in about 27% of CaMKII-positive neurons in the vCA2 area. Because these neurons will not be silenced in the *PCP4-Cre*$^{+/-}$ line we have used, we cannot exclude the possibility that this subpopulation of vCA2 neurons is important for SNRM. Nonetheless, our approach does allow us to target the majority of vCA2 pyramidal cells and we find that this targeting is sufficient to almost completely suppress social aggression, similar to the effect of silencing the more homogeneous population of dCA2 neurons with *Cre* lines.

Finally, at present, we lack a specific molecular marker that enables the unambiguous discrimination of vCA2 PNs from surrounding vCA1 and vCA3 neurons. Moreover, we lack a molecular marker that is uniquely expressed in vCA2 neurons compared with dCA2 neurons. As a result, the precise borders of vCA2 along either the longitudinal or transverse axes are uncertain. Future work using single-cell RNA-seq and/or spatial transcriptomics will be needed to explore further the patterns of molecular expression and functional role of CaMKII-positive PNs in the vCA2 region.

RESOURCE AVAILABILITY

Lead contact

Further information and requests for resources and reagents should be directed to and will be fulfilled by the lead contact, Steven Siegelbaum (sas8@cumc.columbia.edu).

Materials availability

This study did not generate new materials.

Data and code availability

- All animal data reported in this paper will be made available upon request by the lead contact.
- No original code was generated in the analysis of this study.
- Any additional information required to reanalyze the data reported in this paper is available from the lead contact upon request.

ACKNOWLEDGMENTS

This work was supported by F30 MH120922-01 (L.M.B.) and grants R01-MH104602 and R01-MH116190 from NIH (PI, S.A.S.). Portions of the study were also supported by a grant from the Zegar Family Foundation.

AUTHOR CONTRIBUTIONS

L.M.B. and S.A.S. conceived the project. L.M.B., W.S., F.L., and S.A.S. designed the experiments. L.M.B., W.S., F.L., R.S., S.I., and A.V. collected the data, and L.M.B. and W.S. analyzed the data. H.-J.L. conceived of and generated the *Avpr1b-Cre*$^{+/-}$ mouse line with guidance from W.S.Y. The data were interpreted by L.M.B., W.S., and S.A.S., who wrote the paper with feedback from F.L., R.S., S.I., and A.V.

DECLARATION OF INTERESTS

The authors have no competing interests to report.

STAR★METHODS

Detailed methods are provided in the online version of this paper and include the following:

- KEY RESOURCES TABLE
- EXPERIMENTAL MODEL AND STUDY PARTICIPANT DETAILS
  - Animals
- METHOD DETAILS
  - Immunofluorescent labeling & imaging
  - Avpr1b-Cre$^{+/-}$ x Ai14 labeling
  - *PCP4*-Cre$^{+/-}$ mouse line validation for vCA2-specific expression
  - Cell counting
  - iDISCO brain clearing and light sheet microscope imaging
  - In situ hybridization and RNAscope
  - Viral injection
  - Dual-injection tracing experiment
  - Pharmacogenetic silencing of ventral CA2
  - Dorsal and ventral CA2 silencing
  - Behavior animals
  - Social recall test
  - Social discrimination test
  - *Avpr1b-Cre*$^{+/-}$ and *PCP4-Cre*$^{+/-}$ mice expression validation
  - Social aggression
  - Social preference test
  - Olfactory habituation/dishabituation
  - *In vitro* electrophysiology and data analysis
- QUANTIFICATION AND STATISTICAL ANALYSIS

SUPPLEMENTAL INFORMATION

Supplemental information can be found online at https://doi.org/10.1016/j.celrep.2025.115714.

Received: July 22, 2024
Revised: February 18, 2025
Accepted: April 25, 2025
Published: May 13, 2025

REFERENCES

1. Lorente de Nó, R. (1934). Studies of the structure of the cerebral cortex. II. Continuation of the study of the ammonic system. J. Psychol. Neurol. *46*, 113–177.
2. Fanselow, M.S., and Dong, H.W. (2010). Are the dorsal and ventral hippocampus functionally distinct structures? Neuron *65*, 7–19. https://doi.org/10.1016/j.neuron.2009.11.031.
3. Cembrowski, M.S., Wang, L., Sugino, K., Shields, B.C., and Spruston, N. (2016). Hipposeq: a comprehensive RNA-seq database of gene expression in hippocampal principal neurons. Elife *5*, e14997.
4. Pothuizen, H., Zhang, W., Jonhgen-Relo, A., Feldon, J., and Yee, B. (2004). Dissociation of function between the dorsal and ventral hippocampus in spatial learning abilities of the rat: a within-subject, within-task comparison of reference and working spatial memory. Eur. J. Neurosci. *19*, 705–712.
5. Moser, M., Moser, E., Forest, E., Andersen, P., and Morris, R. (1995). Spatial learning with a minislab in the dorsal hippocampus. Proc. Natl. Acad. Sci. USA *92*, 9697–9701.
6. Kjelstrup, K.G., Tuvnes, F.A., Steffenach, H.A., Murison, R., Moser, E.I., and Moser, M.B. (2002). Reduced fear expression after lesions of the ventral hippocampus. Proc. Natl. Acad. Sci. USA *99*, 10825–10830.
7. Jimenez, J.C., Su, K., Goldberg, A.R., Luna, V.M., Biane, J.S., Ordek, G., Zhou, P., Ong, S.K., Wright, M.A., Zweifel, L., et al. (2018). Anxiety cells in a hippocampal-hypothalamic circuit. Neuron *97*, 670–683.e6.
8. Schumacher, A., Villaruel, F.R., Ussling, A., Riaz, S., Lee, A.C.H., and Ito, R. (2018). Ventral hippocampal CA1 and CA3 differentially mediate learned approach-avoidance conflict processing. Curr. Biol. *28*, 1318–1324.e4.
9. Ciocchi, S., Passecker, J., Malagon-Vina, H., Mikus, N., and Klausberger, T. (2015). Brain computation. Selective information routing by ventral hippocampal CA1 projection neurons. Science *348*, 560–563. https://doi.org/10.1126/science.aaa3245.
10. Milner, B., Corkin, S., and Teuber, H.L. (1968). Further analysis of the hippocampal amnesic syndrome: 14-year follow-up study of H.M. Neuropsychologia *6*, 215–234.
11. Okuyama, T., Kitamura, T., Roy, D.S., Itohara, S., and Tonegawa, S. (2016). Ventral CA1 neurons store social memory. Science *353*, 1536–1541.
12. Chiang, M., Huang, A., Wintzer, M., Ohshima, T., and McHugh, T. (2018). A role for CA3 in social recognition memory. Behav. Brain Res. *354*, 22–30.
13. Lopez-Rojas, J., de Solis, C.A., Leroy, F., Kandel, E.R., and Siegelbaum, S.A. (2022). A direct lateral entorhinal cortex to hippocampal CA2 circuit conveys social information required for social memory. Neuron *110*, 1559–1572.e4.
14. Hitti, F.L., and Siegelbaum, S.A. (2014). The hippocampal CA2 region is essential for social memory. Nature *508*, 88–92.
15. Stevenson, E.L., and Caldwell, H.K. (2014). Lesions to the CA2 region of the hippocampus impair social memory in mice. Eur. J. Neurosci. *40*, 3294–3301.
16. Smith, A., Williams, A.S., Cymerblit-Sabba, A., Song, J., and Young, W.S. (2016). Targeted activation of the hippocampal CA2 area strongly enhances social memory. Mol. Psychiatr. *21*, 1137–1144.
17. Meira, T., Leroy, F., Buss, E.W., Oliva, A., Park, J., and Siegelbaum, S.A. (2018). A hippocampal circuit linking dorsal CA2 to ventral CA1 critical for social memory dynamics. Nat. Commun. *9*, 4163.
18. Oliva, A., Fernández-Ruiz, A., Leroy, F., and Siegelbaum, S.A. (2020). Hippocampal CA2 sharp-wave ripples reactivate and promote social memory. Nature *587*, 264–269. https://doi.org/10.1038/s41586-020-2758-y.
19. Pimpinella, D., Mastrorilli, V., Giorgi, C., Coemans, S., Lecca, S., Lalive, A. L., Ostermann, H., Fuchs, E.C., Monyer, H., Mele, A., et al. (2021). Septal cholinergic input to CA2 hippocampal region controls social novelty discrimination via nicotinic receptor-mediated disinhibition. Elife *10*, e65580. https://doi.org/10.7554/eLife.65580.
20. Cymerblit-Sabba, A., Walsh, C., Duan, K.-Z., Song, J., Holmes, O., and Young, W.S. (2023). Simultaneous Knockouts of the Oxytocin and Vasopressin 1b Receptors in Hippocampal CA2 Impair Social Memory. Preprint at bioRxiv. https://doi.org/10.1101/2023.01.30.526271.
21. Kassraian, P., Bigler, S.K., Gilly Suarez, D.M., Shrotri, N., Barnett, A., Lee, H.J., Young, W.S., and Siegelbaum, S.A. (2024). The hippocampal CA2 region discriminates social threat from social safety. Nat. Neurosci. *27*, 2193–2206. https://doi.org/10.1038/s41593-024-01771-8.
22. Leroy, F., Park, J., Asok, A., Brann, D.H., Meira, T., Boyle, L.M., Buss, E. W., Kandel, E.R., and Siegelbaum, S.A. (2018). A hippocampal CA2 to lateral septal circuit disinhibits social aggression. Nature *564*, 213–218.
23. Rosene, D., and Van Hoesen, G. (1987). The hippocampal formation of the primate brain. Cerebr. Cortex *6*, 345–356.
24. Lein, E.S., Callaway, E.M., Albright, T.D., and Gage, F.H. (2005). Redefining the boundaries of the hippocampal CA2 subfield in the mouse using gene expression and 3-Dimensional Reconstruction. J. Comp. Neurol. *485*, 1–10.
25. Williams Avram, S.K., Lee, H.J., Fastman, J., Cymerblit-Sabba, A., Smith, A., Vincent, M., Song, J., Granovetter, M.C., Lee, S.H., Cilz, N.I., et al. (2019). NMDA Receptor in Vasopressin 1b Neurons Is Not Required for Short-Term Social Memory, Object Memory or Aggression. Front. Behav. Neurosci. *13*, 218. https://doi.org/10.3389/fnbeh.2019.00218.

26. Dudek, S.M., Alexander, G.M., and Farris, S. (2016). Rediscovering area CA2: unique properties and functions. Nat. Rev. Neurosci. *17*, 89–102.

27. Zhao, M., Choi, Y.S., Obrietan, K., and Dudek, S.M. (2007). Synaptic plasticity (and lack therof) in hippocampal CA2 neurons. J. Neurosci. *27*, 12025–12032.

28. Chevaleyre, V., and Siegelbaum, S.A. (2010). Strong CA2 pyramidal neuron synapses define a powerful disynaptic cortico-hippocampal loop. Neuron *66*, 560–572. https://doi.org/10.1016/j.neuron.2010.04.013.

29. Sun, Q., Sotayo, A., Cazzulino, A.S., Snyder, A.M., Denny, C.A., and Siegelbaum, S.A. (2017). Proximodistal Heterogeneity of Hippocampal CA3 Pyramidal Neuron Intrinsic Properties, Connectivity, and Reactivation during Memory Recall. Neuron *95*, 656–672.e3. https://doi.org/10.1016/j.neuron.2017.07.012.

30. Young, W.S., Li, J., Wersinger, S.R., and Palkovits, M. (2006). The Vasopressin 1b Receptor is prominent in hippocampal area CA2 where it is unaffected by restraint stress or adrenalectomy. Neuroscience *143*, 1031–1039.

31. Raam, T., McAvoy, K.M., Besnard, A., Veenema, A.H., and Sahay, A. (2017). Hippocampal oxytocin receptors are necessary for discrimination of social stimuli. Nat. Commun. *8*, 2001. https://doi.org/10.1038/s41467-017-02173-0.

32. Wersinger, S.R., Ginns, E.I., O'Carroll, A.M., Lolait, S.J., and Young, W.S. (2002). Vasopressin V1b receptor knockout reduces aggressive behavior in male mice. Mol. Psychiatry *7*, 975–984.

33. Pagani, J.H., Zhao, M., Cui, Z., Avram, S.K.W., Caruana, D.A., Dudek, S.M., and Young, W.S. (2015). Role of the vasopressin 1b receptor in rodent aggressive behavior and synaptic plasticity in hippocampal area CA2. Mol. Psychiatry *20*, 490–499.

34. Hedge, S., Capell, W., Ibrahim, B., Klett, J., Patel, N.S., Sougiannis, A.T., and Kelly, M.P. (2016). Phosphodiesterase 11A (PDE11A), enriched in ventral hippocampus neurons, is required for consolidation of social but not nonsocial memories in mice. Neuropsychopharmacology *41*, 2920–2931.

35. Bienkowski, M.S., Bowman, I., Song, M.Y., Gou, L., Ard, T., Cotter, K., Zhu, M., Benavidez, N.L., Yamashita, S., Abu-Jaber, J., et al. (2018). Integration of gene expression and brain-wide connectivity reveals the multiscale organization of mouse hippocampal networks. Nat. Neurosci. *21*, 1628–1643. https://doi.org/10.1038/s41593-018-0241-y.

36. Bienkowski, M.S. (2023). Further refining the boundaries of the hippocampus CA2 with gene expression and connectivity: Potential subregions and heterogeneous cell types. Hippocampus *33*, 150–160. https://doi.org/10.1002/hipo.23508.

37. Radzicki, D., Chong, S., and Dudek, S.M. (2023). Morphological and molecular markers of mouse area CA2 along the proximodistal and dorsoventral hippocampal axes. Hippocampus *33*, 133–149. https://doi.org/10.1002/hipo.23509.

38. Renier, N., Wu, Z., Simon, D.J., Yang, J., Ariel, P., and Tessier-Lavigne, M. (2014). iDISCO: a simple, rapid method to immunolabel large tissue samples for volume imaging. Cell *159*, 896–910. https://doi.org/10.1016/j.cell.2014.10.010.

39. Bartesaghi, R., and Ravasi, L. (1999). Pyramidal neuron types in field CA2 of the guinea pig. Brain Res. Bull. *50*, 263–273. https://doi.org/10.1016/s0361-9230(99)00198-7.

40. Helton, T.D., Zhao, M., Farris, S., and Dudek, S.M. (2019). Diversity of dendritic morphology and entorhinal cortex synaptic effectiveness in mouse CA2 pyramidal neurons. Hippocampus *29*, 78–92. https://doi.org/10.1002/hipo.23012.

41. Swanson, L.W., and Cowan, W.M. (1977). An autoradiographic study of the organization of the efferent connections of the hippocampal formation in the rat. J. Comp. Neurol. *172*, 49–84. https://doi.org/10.1002/cne.901720104.

42. Kohara, K., Pignatelli, M., Rivest, A.J., Jung, H.Y., Kitamura, T., Suh, J., Frank, D., Kajikawa, K., Mise, N., Obata, Y., et al. (2014). Cell type-specific genetic and optogenetic tools reveal hippocampal CA2 circuits. Nat. Neurosci. *17*, 269–279.

43. Jamiolkowski, R.M., Nguyen, Q.A., Farrell, J.S., McGinn, R.J., Hartmann, D.A., Nirschl, J.J., Sanchez, M.I., Buch, V.P., and Soltesz, I. (2024). The fasciola cinereum of the hippocampal tail as an interventional target in epilepsy. Nat. Med. *30*, 1292–1299. https://doi.org/10.1038/s41591-024-02924-9.

44. Villegas, A., and Siegelbaum, S.A. (2024). Modulation of aggression by social novelty recognition memory in the hippocampal CA2 region. Preprint at bioRxiv. https://doi.org/10.1101/2024.05.03.592403.

45. Weeden, C.S.S., Roberts, J.M., Kamm, A.M., and Kesner, R.P. (2015). The role of the ventral dentate gyrus in anxiety-based behaviors. Neurobiol. Learn. Mem. *118*, 143–149.

46. Kheirbek, M.A., Drew, L.J., Burghardt, N.S., Costantini, D.O., Tannenholz, L., Ahmari, S.E., Zeng, H., Fenton, A.A., and Hen, R. (2013). Differential Control of Learning and Anxiety along the Dorsoventral Axis of the Dentate Gyrus. Neuron *77*, 955–968.

47. Cui, Z., Gerfen, C.R., and Young, W.S. (2013). Hypothalamic and other connections with dorsal CA2 area of the mouse hippocampus. J. Comp. Neurol. *521*, 1844–1866. https://doi.org/10.1002/cne.23263.

48. Robert, V., Therreau, L., Chevaleyre, V., Lepicard, E., Viollet, C., Cognet, J., Huang, A.J., Boehringer, R., Polygalov, D., McHugh, T.J., and Piskorowski, R.A. (2021). Local circuit allowing hypothalamic control of hippocampal area CA2 activity and consequences for CA1. Elife *10*, e63352. https://doi.org/10.7554/eLife.63352.

49. Boyle, L.M., Posani, L., Irfan, S., Siegelbaum, S.A., and Fusi, S. (2024). Tuned geometries of hippocampal representations meet the computational demands of social memory. Neuron *112*, 1358–1371.e9. https://doi.org/10.1016/j.neuron.2024.01.021.

50. Donegan, M.L., Stefanini, F., Meira, T., Gordon, J.A., Fusi, S., and Siegelbaum, S.A. (2020). Coding of social novelty in the hippocampal CA2 region and its disruption and rescue in a 22q11.2 microdeletion mouse model. Nat. Neurosci. *23*, 1365–1375. https://doi.org/10.1038/s41593-020-00720-5.

51. Krashes, M.J., Koda, S., Ye, C., Rogan, S.C., Adams, A.C., Cusher, D.S., Maratos-Flier, E., Roth, B.L., and Lowell, B.B. (2011). Rapid, reversible activation of AgRP neurons drives feeding behavior in mice. J. Clin. Investig. *121*, 1424–1428. https://doi.org/10.1172/JCI46229.

52. Oh, S.W., Harris, J.A., Ng, L., Winslow, B., Cain, N., Mihalas, S., Wang, Q., Lau, C., Kuan, L., Henry, A.M., et al. (2014). A mesoscale connectome of the mouse brain. Nature *508*, 207–214. https://doi.org/10.1038/nature13186.

53. Sheng, W., Harden, S.W., Tan, Y., Krause, E.G., and Frazier, C.J. (2021). Dendritic osmosensors modulate activity-induced calcium influx in oxytocinergic magnocellular neurons of the mouse PVN. Elife *10*, e63486. https://doi.org/10.7554/eLife.63486.

STAR★METHODS

KEY RESOURCES TABLE

REAGENT or RESOURCE	SOURCE	IDENTIFIER
Antibodies		
Rabbit anti-PCP4	Sigma-Aldrich	#HPA005792; RRID:AB_1855086
Mouse anti-RGS14 (IgG2a)	Neuromab	#75–170; RRID:AB_2179931
Mouse anti-STEP (IgG1)	Cell Signaling Technology	#4396; RRID:AB_1904101
Rabbit anti-RFP	Rockland	#600-401-379; RRID: AB_2209751
Chicken anti-GFP	Aves	#GFP-1010; RRID: AB_2307313
Mouse IgG1 anti-CaMKII alpha	Abcam	#ab22609; RRID:AB_447192
Bacterial and virus strains		
AAV2/8 hSyn.DIO.hM4D(Gi)-mCherry	Krashes et al.[51]	Addgene AAV2/8; 44362-AAV8
AAV9.CAG.FLEX.eGFP.WPRE.HGH	Oh et al.[52]	Addgene AAV9; 51502-AAV9
AAV9.EF1a.dflox.hChR2(H134R).EYFP. WPRE.HGH	Deisseroth (unpublished)	Addgene AAV9; 20298-AAV9
AAV2.EF1a.DIO.mCherry	Penn Vector Core	Addgene_50462
AAV9.EF1a.dflox.hChR2(H134R). mCherry. WPRE.HGH	Deisseroth (unpublished)	Addgene AAV9; 20297-AAV9
Experimental models: Organisms/strains		
Avpr1b-Cre$^{+/-}$ mice (B6.Cg-*Avpr1b*$^{tm2.1(cre)Wsy}$/J)	Jacson Laboratory; Young Laboratory	Strain #036876; RRID: IMSR_JAX:036876
PCP4-Cre$^{+/-}$ mice (B6.Cg-Pcp4<tm2.1 (cre)> (RBRC05662))	Takemori, RIKEN Center for Allergy and Immunology	BRC No RBRC05662
Ai14 reporter mice (B6.Cg-Gt(ROSA) 26Sortm9(CAG-tdTomato)Hze/J)	Jackson Laboratory	Strain # 007909, RRID: IMSR_JAX:007914
Software and algorithms		
ANY-maze	Stoelting Co.	https://stoeltingco.com/Neuroscience/Anymaze/Any-maze-Video-Tracking/Any-maze-Software
PRISM	Graphpad	https://www.graphpad.com/scientific-software/prism/
Fiji	ImageJ	https://imagej.net/software/fiji/
Imaris	Oxford Instruments	https://imaris.oxinst.com/
OriginLab	OriginLab Corporation	https://www.originlab.com/
pClamp 10	Molecular Devices	https://www.moleculardevices.com/products/axon-patch-clamp-system/acquisition-and-analysis-software/pclamp-software-suite

EXPERIMENTAL MODEL AND STUDY PARTICIPANT DETAILS

Animals

All mouse procedures were performed in accordance with the NIH guidelines and with the approval of the Columbia University Institutional Animal Care and Use Committee. Mice were housed with littermates unless otherwise noted and kept on a 12-h light-dark cycle in air-filtered, temperature- and humidity-controlled conditions with food and water available *ad libitum*. Experiments were carried out on 2 to 6 months old male and female *Avpr1b*-Cre$^{+/-}$ and Cre$^{-/-}$ littermates and male *PCP4*-Cre$^{+/-}$ and Cre$^{-/-}$ littermates.

METHOD DETAILS

Immunofluorescent labeling & imaging

We perfused subject mice using saline followed by 4% PFA in ice-cold PBS. Brains were extracted and incubated in 4% PFA overnight. Brains were sliced in coronal, horizontal, or transverse orientation as specified with thickness of 60 μm using a Leica VT1000S

vibratome. Post-hoc immunohistochemistry of *in vitro* electrophysiological experiments was performed by fixing 400 mm slices in 4% PFA at 4°C overnight. Sections were permeabilized and blocked for 1 h with 5% goat serum and 0.4% Triton X- in PBS at room temperature. Sections were incubated overnight unless otherwise specified with the primary antibodies specified below at 4°C in 0.1% Triton X- in PBS plus 5% goat serum. The following day, slices were washed with PBS three times for 10 min in PBS and then incubated with secondary antibodies (all at concentration 1:500) for 3 h. Slices were again washed three times in PBS for 10 min/wash. DAPI (ThermoFisher Scientific, #D1306) staining was applied at 1:1000 for 15 min in PBS at room temperature prior to mounting. Slices were mounted using Fluoromount (Sigma-Aldrich) and imaged using Zeiss LSM 700 confocal microscope.

Avpr1b-Cre$^{+/-}$ x Ai14 labeling

Brains were dissected to extract the hippocampus from both hemispheres. The hippocampus was sliced in a transverse orientation. To get the complete series of expression, every third slice along the dorsoventral axis was selected for imaging. For quantification of prototypical CA2 marker expression, dorsal and ventral transverse slices were incubated with the following primary and secondary antibody combinations using the protocol described: PCP4 (1:300, rabbit anti-PCP4 #HPA005792, Sigma-Aldrich)/goat anti-rabbit IgG (Life Technologies) and either STEP (*n*-4, 1:1000, mouse anti-STEP # 4396, Cell Signaling Technology)/goat anti-mouse IgG1 (Life Technologies) or RGS14 (*n* = 3, 1:500, mouse anti-RGS14 #75–170, Neuromab)/goat anti-mouse IgG2a (Life Technologies).

PCP4-Cre$^{+/-}$ mouse line validation for vCA2-specific expression

The *PCP4-Cre*$^{+/-}$ mouse line (B6.Cg-Pcp4<tm2.1(cre)> (RBRC05662)) was developed by Toshitada Takemori and provided by RIKEN BRC through the National BioResource Project of the MEXT/AMED, Japan. The hippocampus was extracted from both hemispheres and sectioned in a transverse orientation (*n* = 2). For the dual-labeling of Cre and PCP4, guinea pig anti-Cre (1:4000, Zuckerman Institute antibody core) and rabbit anti- PCP4 (1:300, #HPA005792, Sigma-Aldrich) were used as the primary antibodies. Goat anti-guinea pig IgG-555 (1:500, # A-21435, Life Technologies) and goat anti-rabbit IgG-488 (1:500, # A-11008, Life Technologies) were used as the secondary antibodies.

Cell counting

For basic quantification of CA2 markers in dorsal and ventral hippocampus, we chose transverse slices from the last 1/3 of the hippocampus (mouse *n* = 5, slice *n* = 7) and dorsal slices from the first 1/3 of the hippocampus (mouse *n* = 7, slice *n* = 8). The following coordinates were used to define CA2 across slices: from the tip of the mossy fiber, as visualized with PCP4 labeling of the mossy fibers, the lower edge of the area was defined as a 205 μm line lying along the lower edge of the pyramidal layer toward the DG. The deep-to-superficial edge of the area on the CA3-side was defined as 110 μm centered in the middle pyramidal layer. Finally, the upper edge of the area was defined by a 325 μm line moving toward CA1 from the defined CA3 border. 5 consecutive z stack images with a delta of 2.04 μm were selected, for a final volume of 237,864 μm3/slice. These boundaries are consistent with a conservative estimate of CA2 transverse width in line with previous reports.[24]

iDISCO brain clearing and light sheet microscope imaging

Avpr1b-Cre$^{+/-}$ x *Ai14* brains (*n* = 3) were processed as previously described.[38] tdTomato expression was identified using the primary antibody rabbit anti-RFP (1:1000, Rockland, #600-401-379). Background labeling was captured with chicken anti-GFP (1:2000, AVES Labs, #GFP-1020) for 7 days followed by the following respective secondary antibodies: donkey anti-rabbit conjugated to Alexa 488 (1:1000, Thermo Fisher Scientific, # A-21206) and donkey anti-chicken conjugated to Alexa 647 (1:2000, Jackson #703-605-155) for 7 days. Light sheet microscopy was performed using an UltraMicroscope II light-sheet microscope (LaVision). 3-D reconstruction was completed via Imaris software (Bitplane).

In situ hybridization and RNAscope

Brain collection

Brains were dissected from *Avpr1b-Cre*$^{+/-}$ mice crossed to an *Ai14* background to express tdTomato in Avpr1b-expressing cells (*n* = 2) and immersed in dry-ice cold Butan X to freeze for 6 s. Frozen brains were embedded in OCT and sliced coronally in 16 μm sections using a Leica CM3050 S cryostat. Slices were mounted onto Superfrost Plus slides (12-550-15, FisherBrand). Sections were moved to a −20°C fridge to dry and then stored in an air tight wrapped slide box at −80°C.

Pre-assay tissue preparation

To prepare slices, slides were immersed in 10% NBS for 15 min at 4°C. Slides were then transferred to wash in different EtOH concentrations for 5 min each at room temperature (RT): 50%, 70%, 100%, 100%. Slices were removed and placed on absorbent paper to dry for 5 min. An ImmEdge hydrophobic barrier pen was used to draw a barrier around the slices. A HybEZ II Hybridization System oven (Advanced Cell Diagnostics) was set to −40°C. Dried slides were places on the HybEZ slide rack and 4 drops of protease IV was added per section and allowed to incubate at RT for 30 min. Liquid was removed and the slides were immediately places in a tissue tek slide rack in a tissue tek staining dish filled with 1x PBS, and this process was repeated 1x time.

Fluorescent RNAscope assay

Avpr1b and *tdTomato* probes (Advanced Cell Diagnostics RNAscope Probes Cat #480141 and 317041, respectively) were warmed to 40°C for 10 min and then cooled to RT. Probes were spun down and then mixed at a ratio of 1:50 (*Avpr1b*: *tdTomato*). Excess liquid

was removed from slides and 4 drops of the probe were added to the slides. Slides were placed in the HybEZ oven tray and secured in the oven. They were incubated for 2 h at 40°C. Slides were then removed, tapped to remove excess fluid, and immersed in 1x wash buffer for 2 min at RT twice. For each AMP, excess fluid was removed from the slide and then 4 drops were added proceeding from 1 to 4. Slides were placed in the HybEZ oven tray and incubated with the following times: 1: 30 min, 2: 15 min, 3: 30 min, 4: 15 min. Following AMP4, slides were immersed in 1x wash buffer for 2 min at RT twice. Excess fluid was removed by tapping slide and 4 drops DAPI was added to slides. Slides were incubated for 1 min at room temperature. DAPI was removed and immediately Prolong Gold Antifade (w/o DAPI) was added to the slide and cover-slipped. Slides were stored in dark at 4°C until they were imaged using a Zeiss LSM 700 confocal microscope.

Viral injection

Subject mice were given 5 mg/kg carprofen analgesic and anesthetized with 2–5% isoflurane. Subjects were placed in a stereotaxic frame and a craniotomy was drilled at the target coordinates. A glass pipette containing the virus was lowered to the desired depth. A Nano-Inject II (Drummond Scientific) was used to inject 23 nL virus at intervals of 10 s to obtain the desired volume. Following injection, 5 min were allowed to pass before the pipette was retracted. All viral injection coordinates are in mm with bregma as reference.

Dual-injection tracing experiment

Avpr1b-Cre$^{+/-}$ subject mice (n = 4) were injected in dCA2 (AP -2.0, ML $^{+/-}$1.8, DV -1.7) with 200 nL of either: AAV9.CAG.FLEX.eGFP.WPRE.HGH (1x10°12 pp/mL, UPenn Vector Core, cohort 1, n = 2) or AAV9.EF1a.dflox.hChR2(H134R).EYFP.WPRE.HGH (1x10°12 pp/mL, Addgene, cohort 2, n = 2). Subject mice were additionally injected in vCA2 (AP -3.0, ML $^{+/-}$3.2, DV -3.8) with 200 nL of either: AAV2.EF1a.DIO.mCherry (1x10°12 pp/mL, UPenn Vector Core, cohort 1) or AAV9.EF1a.dflox.hChR2(H134R).mCherry.WPRE.HGH (1x10°12 pp/mL, Addgene, cohort 2). We observed no difference in the projection patterns between cohorts. Cohort 1 was injected unilaterally in the right hemisphere; cohort 2 was injected bilaterally. Single-injection tracing experiment: *Amigo2-Cre*$^{+/-}$ subject mouse (n = 1) was injected in vCA2 (AP -3.0, ML $^{+/-}$3.2, DV -3.8) with 200 nL AAV9.EF1a.dflox.hChR2(H134R).mCherry.WPRE.HGH (1x10°12 pp/mL, Addgene). For subjects in cohort 1 (n = 2), brains were extracted and sliced in a coronal orientation. For cohort 2 (n = 2), brains were extracted and divided into three parts by 2 slices: 1) a coronal slice at the intersection of the hippocampus and the lateral septum separating the brain into an anterior and posterior portion, and 2) a slice in the posterior portion separating the two hemispheres. The anterior portion was sliced in a horizontal orientation to observe projections to the lateral septum. The hippocampus from the right hemisphere was extracted and sliced in a transverse orientation. The posterior portion from the left hemisphere was sliced in a horizontal orientation. Through this method, we were able to visualize the projections from dorsal and ventral hippocampus both outside the hippocampus in coronal and horizontal sections, and within the hippocampus in coronal, horizontal, and transverse sections.

Viral tracing, single injection: The hippocampus was dissected from both hemispheres of the Amigo2-Cre mouse brain. The hippocampus was sliced in a transverse orientation and then stained for PCP4 (1:300, rabbit anti-PCP4 #HPA005792, Sigma-Aldrich) as primary and goat anti-rabbit IgG (Life Technologies), for secondary.

Pharmacogenetic silencing of ventral CA2

Avpr1b-Cre$^{+/-}$ and Cre$^{-/-}$ littermates or *PCP4*-Cre$^{+/-}$ and Cre$^{-/-}$ littermates were injected with a Cre-dependent AAV expressing the inhibitory hM4Di designer receptor exclusively activated by designer drugs (iDREADD) (200 nL bilaterally at 1.9x10°12 pp/ml with AAV2/8 hSyn.DIO.hM4D(Gi)-mCherry] bilaterally at coordinates for dorsal CA2 (AP -2.0, ML $^{+/-}$1.8, DV -1.7) or ventral CA2 (AP -3.0, ML $^{+/-}$3.2, DV -3.8).

Dorsal and ventral CA2 silencing

Three weeks post-injection, subject mice were habituated to saline intraperitoneal injections 4 days prior to testing, alternating the side of injection each day. One day prior to testing, subjects were weighed to ensure proper CNO dosage. CNO solution (Cayman Pharmaceuticals, CAS # 34233-69-7) was mixed on day of the experiment to reach a concentration of 1 mg/mL in sterile saline. 30-min prior to each test, intraperitoneal injections of subject mice were performed with a volume to ensure 10 mg/kg CNO dose unless otherwise specified. Subjects and any stimuli mice were moved to the testing area 30 min prior to the experiment start to habituate to the test room. Stimulus mice were always sex- and age-matched. Videos of experiments were recorded using a FireWire camera (DMK 31AF03-Z2; The Imaging Source) triggered through ANY-maze software.

Behavior animals

We used both male and female *Avpr1b-Cre*$^{+/-}$ mice (and *Cre*$^{-/-}$ littermate controls) in social memory tests. We found no significant differences in social memory between male and females in either group (two-way ANOVA genotype x interaction partner $F(3,19) = 0.07945$, $p = 0.97$; interaction partner $F(1,19) = 10.06$, $p = 0.0050$. Šídák's multiple comparisons *Avpr1b-Cre*$^{+/-}$ females vs. *Avpr1b-Cre*$^{+/-}$ males, $p > 0.99$.). For resident-intruder tests of aggression we used only males, as females are known to show little aggression in this test. Studies on aggression used *PCP4*-Cre$^{+/-}$ and Cre$^{-/-}$ male littermates. Male mice were also used exclusively in social memory tests with the *PCP4*-Cre$^{+/-}$ and Cre$^{-/-}$ littermates to enable a direct comparison of CA2 silencing results in the same subjects in the two social behaviors (memory and aggression). Behavior was run under low red-light conditions unless otherwise specified. All behavior experiments were recorded with ANY-maze software.

Social recall test

One day prior to testing, subjects were habituated to the arena, a three-chambered box with each chamber measuring 19 cm × 40.5 cm x 22 cm. The apparatus was made of clear Plexiglass with openings 10 cm side to allow access across chambers. Within the arena, two empty pencil cups (radius 5 cm) were placed in each of the side chambers. Following 10 min habituation, subjects were returned to their home cages. On the test day, following CNO injection, subject mice and littermates were separated into two testing cages at random (A or B) and brought to the test room. Stimulus mice, with whom the subject mice had never interacted, were also brought to the test room to habituate. After 30-min, the subject mice were introduced to the central chamber of the three-chamber apparatus with two barriers blocking the doorways to the side chambers, which each held an empty pencil cup. The barriers were removed to start the test, and the subject mice freely explored the three chambers for 10 min. The mouse was again confined to the central chamber. A littermate from the opposite testing cage was placed under the pencil cup in one chamber, and a novel stimulus mouse was placed under the pencil cup in the opposite chamber. The location of the novel and littermate mouse was alternated across mice. The barriers were again removed, and the subject allowed to explore the novel conspecific and familiar littermate freely for 10 min. The time spent in each chamber was measured automatically using zones defined within ANY-maze.

Social discrimination test

One day prior to testing, mice were habituated to an oval arena that consisted of two half-circles with radius 15cm connected to a central square area with length of 30 cm (dimensions: length 60 cm, width 30 cm, height 45 cm). Wire pencil cups (radius 5 cm) were placed 10 cm from the two ends of the arena along the midline. Following 10-min habituation, subjects were returned to their home cages. The next day following CNO injection and 30-min habituation to the testing room, subjects were re-introduced to the oval arena with empty pencil cups for 5 min. The subject was removed and returned to their home cage, and two stimulus mice were placed into the arena, with one under each pencil cup. The subject mouse was returned to the arena and allowed to freely interact with these individuals for 5 min. The subject mice were then returned to their home cage for 30 min. The subject was then returned to the oval arena with the empty pencil cups for 5 min. The subject was again removed to their home cage, and two stimulus mice (one from the prior trial and a third novel individual) were placed at random under each of the two pencil cups. The subject mouse was again returned to the arena and allowed to investigate the now-familiar and novel individual freely for 5 min. The time in a circular zone (radius = 10cm) around each cup was automatically scored.

Avpr1b-Cre$^{+/-}$ and *PCP4-Cre*$^{+/-}$ mice expression validation

For dCA2 pharmacogenetic silencing, *Avpr1b-Cre*$^{+/-}$ mouse brains were sliced coronally to allow all dorsal hippocampal subfields to be simultaneously imaged. For vCA2 pharmacogenetic silencing, *Avpr1b-Cre*$^{+/-}$ or *PCP4*-Cre$^{+/-}$ mouse brains were sliced horizontally to allow all ventral hippocampal subfields to be simultaneously imaged. Brains were incubated with the following primary/secondary antibody pairing: PCP4 (1:300, rabbit anti-PCP4 #HPA005792, Sigma-Aldrich)/goat anti-rabbit IgG (Life Technologies). Mice with low levels of expression (<50% Avpr1b-expressing CA2 PNs infected in *Avpr1b-Cre* mice or <50% infection of DAPI+ cells in vCA2 region in *PCP4*-Cre$^{+/-}$ mice) or significant expression outside of CA2 (>10% florescent expression of the areas of CA1, CA3 or DG with a binary mask in *PCP4*-Cre$^{+/-}$ mice). Due to the absence of an Avpr1b antibody, to confirm co-expression with iDREADD, we used a PCP4 antibody to label vCA2. As noted in the text, we expect two major populations of vCA2 neurons: PCP4-positive/Avpr1b-positive (59.8 ± 7.5%) and PCP4-only (36.6 ± 6.0%). Thus, we expect roughly 59.8% of PNs infected in the *Avpr1b-Cre*$^{+/-}$ mouse to express the iDREADD virus. Therefore, mice with <29.9% expression of iDREADD (50% of the Avpr1b-expressing population) in vCA2 from either hemisphere were excluded from analysis in experiments in which the *Avpr1b-Cre*$^{+/-}$ subjects were used.

Social aggression

PCP4-Cre$^{+/-}$ male mice and their Cre$^{-/-}$ littermates were bilaterally injected with AAV8-hm4Di-mCherry into the vCA2. After 8 days of recovery, the mice were singly housed for 10 days before the social aggression test. The resident-intruder paradigm was adjusted based on previously published experiments.[22] Stimulus mice (7-8 week-old BALB/cByJ male intruders) were group housed and used only once per day. On the aggression screening days, the subject mice were first received a saline injection (5 mL/kg, ip) as a control for the test day. After a 30-min room habituation, stimulus mice were introduced to the home cages of the subject mice for 5-min free interaction. In accordance with Columbia IACUC rules, the attack was allowed to continue for 1 min after its onset, which was defined by a clear bite. To increase the occurrences of aggression and select the aggressive subjects, 3 continuous days of screenings were allowed for each subject (19–21 days after the virus injections). On the test day, CNO (5 mg/kg, ip; 5 mg/kg dosing was also used in social memory experiments with *PCP4*-Cre mice to match dosing in aggression experiments) was injected 30 min prior to the test. A 10-min resident-intruder test was then performed with a novel intruder introduced to the home cage of the PCP4-Cre subject mice. ANY-maze software (Stoelting Company) was used for recording and measurements.

Social preference test

Subjects were habituated 1 day prior to testing to a square opaque white arena (dimensions 50 cm × 50 cm). Test day, mice were injected with CNO and brought to habituate to the testing room for 30-min. Subjects were then introduced to the empty square arena for 5 min. The subject was temporarily removed from the chamber. An empty wire pencil cup (radius 5 cm) was placed in one corner

and a pencil cup (radius 5 cm) with a stimulus mouse was placed in the opposite corner. Subject mice were returned to the chamber and allowed to freely explore the arena for 10 min. Between mice and between habituation and testing, the square arena was cleaned with 70% propan-2-ol wipes (VWR) and allowed to air-dry for 2 min. Following testing, videos were automatically scored using ANY-maze software as defined by time spent in two square interaction zones (20 × 20 cm) originating from the corners of the arena in which the stimulus were placed.

Olfactory habituation/dishabituation

Mice were habituated to a novel cage filled with bedding for 5 min. A series of cue tips dipped in odors were introduced through the cage lid approximately 4.5 cm deep for 2 min each, as described in (Yang and Crawley 2009). After 2 min, the cue tip was removed from the cage and replaced with a cue tip dipped in another odor. The same odor was introduced three times in a row with a new cue tip each 156 presentation. The following odors were introduced (in order), concentrations in parentheses: deionized water, almond (1:100), banana (1:100), social mouse A, social mouse B. For social odors, the cue tip was dipped in deionized water and then moved in a zigzag through mouse bedding from two different cages (A and B). Social odors were from sex- and age-matched mouse cages with which the subject had no prior experience. Investigation time with the cue tip was manually scored by a blinded investigator across trials.

In vitro electrophysiology and data analysis

In vitro electrophysiology was performed in the 8-16 week-old male and female *Avpr1b-Cre*$^{+/-}$ x *Ai14* mice and *Avpr1b-Cre*$^{+/-}$ mice. Mice were anesthetized by isoflurane inhalation and transcardially perfused with ice-cold sucrose ACSF containing, in mM: 195 sucrose, 10 glucose, 25 NaHCO3, 2.5 KCl, 1.25 NaH2PO4, 2 sodium pyruvate, 0.5 CaCl2, 7 MgCl2. Mice were then decapitated and hippocampi were quickly dissected in the sucrose ACSF, placed into a 4% agar mold, and sectioned into 400 μm transverse slices with a vibratome (VT1200S, Leica). Slices were then transferred into a warmed (32°C) recovery beaker containing 50% sucrose ACSF and 50% ACSF (2.5 glucose, 125 NaCl, 25 NaHCO3, 2.5 KCl, 1.25 NaH2PO4, 3 sodium pyruvate, 1 ascorbic acid, 2 CaCl2, and 1 MgCl2) for recovery. After at least 30 min of incubation, the beaker was kept in room temperature for an additional 30 min prior to recording. All the solutions were continuously saturated with carbogen gas (95% O2/5% CO2).

Recording pipettes and stimulation pipettes were prepared with borosilicate glass capillaries using a heated-filament puller with an open tip resistance of 3–6 MΩ when filled with an intracellular solution containing, in mM: 135 potassium gluconate, 5 KCl, 0.2 EGTA, 10 HEPES, 2 NaCl, 5 MgATP, 0.4 Na2GTP, 10 Na2phosphocreatine, and biocytin (0.2% by weight), adjusted to pH 7.2 and osmolarity 295 mOsm. For voltage-clamp recordings of slice optogenetic experiments, KCl was replaced with cesium methanesulfonate in the intracellular solution. Whole cell recordings were acquired using a Multiclamp 700A amplifier (Molecular Device), data acquisition interface ITC-18 (Instrutech) and pClamp 10. The CA1/CA2 border was identified as the end of the stratum lucidum (SL) and the edge of Cre-dependent fluorescence marker expression. PNs were identified based on the cellular morphology and intrinsic properties such as the absence of fast spiking. Access resistance (15–25 MΩ) was continuously monitored.

Membrane capacitance was obtained at −70mV from a V-shape voltage clamp ramp protocol with ΔV = ±10 mV. Input resistance was calculated from a voltage step from −70 mV to −80 mV in voltage clamp configuration. Voltage sag was measured with a negative current step initiated from −70 mV in which the steady hyperpolarization potential was between −97 mV and −103 mV. Sag ratio was calculated as (V_{peak}-V_{stt})/(V_{peak}-70 mV, where V_{peak} is the minimum potential at the beginning of the step and V_{stt} is the steady hyperpolarization potential at the end of the step. Rheobase current and action potential properties were calculated with a 1000 pA, 1-s current ramp initiating from −70 mV. For the experiments involving optogenetic activation of CA2 neurons, *Avpr1b-Cre*$^{+/-}$ mice were injected with either AAV8-EF1a-DIO-hChR2(H134R)-mCherry (Addgene, #20297, 200nL bilaterally at 10°12 pp/mL) targeting ventral CA2 (AP -3.0, ML $^{+/-}$3.2, DV -3.8), or AAV5-EF1a-DIO-hChR2(H134R)-eYFP (Addgene, #20298, 200nL bilaterally at 10°12 pp/mL) targeting dorsal CA2 (AP -2.0, ML $^{+/-}$1.8, DV -1.7) three weeks prior to the experiments. During the experiments, photostimulation was delivered as a 2-ms pulse of 470 nm light with an LED light source (ThorLabs High-power 5-channel LED driver with pulse modulation, model DC2100) through a 40x immersion objective with the recorded cell centered in the illumination field. For voltage-clamp recording, cells were clamped at −75 mV (for EPSCs), −70 mV (for contingency of success rate), and +5 mV (for IPSCs). For current clamp recording, cells were initially held at −70 mV. Extracellular electrical stimulation was generated as a 2-ms pulse. The following drugs were bath-applied at the following concentrations: SR 95531 (1 μM, Tocris, #1262), CGP 55845 (2 μM,Tocris, #1248).

To verify the location and the morphology of recorded neurons, all acute hippocampal slices were fixed, permeabilized and blocked for biocytin labeling at the conclusion of recordings. Biocytin was visualized by incubating hippocampal slices with Alexa Fluor 647-conjugated streptavidin (1:1000, Invitrogen#S21374).

QUANTIFICATION AND STATISTICAL ANALYSIS

PRISM (Graphpad) was used for data analysis for behavioral testing. For electrophysiological recordings, data analysis was performed using custom software written in OriginC[53] (OriginLab Corporation, Northampton, MA) and PRISM (Graphpad).[53]